

Research report

Altered GABAergic function accompanies hippocampal degeneration in mice lacking ClC-3 voltage-gated chloride channels

Linda W. Dickerson^{a,e,1}, Daniel J. Bonthius^{a,c,d,g,1}, Brian C. Schutte^{a,f,1}, Baoli Yang^{b,1}, Thomas J. Barna^a, Melissa C. Bailey^a, Keith Nehrke^h, Roger A. Williamson^b, Fred S. Lamb^{a,*}

^aDepartment of Pediatrics, University of Iowa, Iowa City, IA, USA

^bDepartment of Obstetrics and Gynecology, University of Iowa, Iowa City, IA, USA

^cDepartment of Neurology, University of Iowa, Iowa City, IA, USA

^dDepartment of Anatomy and Cell Biology, University of Iowa, Iowa City, IA, USA

^eCardiovascular Research Center, University of Iowa, Iowa City, IA, USA

^fPh.D. Program in Genetics, University of Iowa, Iowa City, IA, USA

^gPh.D. Program in Neuroscience, University of Iowa, Iowa City, IA, USA

^hCenter for Oral Biology, University of Rochester, Rochester, NY, USA

Accepted 27 August 2002

Abstract

Mice lacking ClC-3 chloride channels, encoded by the *Clcn3* gene, undergo neurodegeneration of the hippocampal formation and retina [Neuron, 29 (2001) 185–196; Genes Cells, 7 (2002) 597–605]. We independently created a mouse lacking the *Clcn3* gene which demonstrated similar central nervous system abnormalities, including early postnatal degeneration of retinal photoreceptors. However, we observed a characteristic spatial–temporal sequence of hippocampal neurodegeneration that differs from the pattern previously reported. Anterior-to-posterior degeneration and astrogliosis of the dentate gyrus and hippocampus progressed over months. Sequential loss of hippocampal neuronal subpopulations began in the dentate gyrus and progressed to CA3, followed by CA1 neurons. Projection neurons of the entorhinal cortex degenerated, secondary to the loss of their synaptic targets within the hippocampal formation. Other characteristics of the *Clcn3*^{−/−} mice included an abnormal gait, kyphosis, and absence of hindlimb escape extension upon tail elevation. Spontaneous seizures were observed in four adult *Clcn3*^{−/−} mice, and one mouse died during the event. We hypothesized that neuronal injury may be related to recurrent seizures. *Clcn3*^{−/−} mice had normal serum electrolytes and pH, and exhibited neither hyperglycemia nor rebound hypoglycemia following a glucose load. They displayed a greatly reduced susceptibility to pentylenetetrazole-induced seizures and an abnormally prolonged sedation to benzodiazepines. There was no change in vulnerability to kainic acid-induced seizures. Immunostaining revealed a progressive loss of GABA synthesizing cells in the dentate gyrus. The death of these cells was preceded by increased GABA_A receptor immunoreactivity. These data suggest that GABA_A inhibitory neurotransmission is altered in *Clcn3*^{−/−} mice. The increase in GABA_A receptor density may represent a compensatory response either to chronic excessive excitatory stimuli or reduced inhibitory input from local GABAergic interneurons within the dentate gyrus.

© 2002 Elsevier Science B.V. All rights reserved.

Keywords: Gene targeting; Hippocampus; Pentylenetetrazole; Kainic acid; Midazolam; Glucose tolerance

1. Introduction

Neuronal excitability is modified by chloride ion homeo-

stasis. The concentration gradient for chloride across the cell membrane is determined by the balance of chloride importation (Na–K–2Cl co-transporter, NKCC1) and exportation (KCl co-transporter, KCC2) [52,61], and by the activity of a variety of chloride conductances, including ligand-gated (GABA and glycine), and voltage-gated (ClC family) chloride channels [26]. The effect of chloride channel activation on membrane potential depends on the chloride equilibrium potential of the cell, which varies

*Corresponding author. Department of Pediatrics, 5040-B RCP, 200 Hawkins Drive, Iowa City, IA 52242, USA. Tel.: +1-319-351-0701; fax: +1-319-353-8957.

E-mail address: fred-lamb@uiowa.edu (F.S. Lamb).

¹These authors contributed equally to this study.

among neuronal populations. In adult hippocampal pyramidal neurons, under normal conditions, net outward Cl^- transport makes the equilibrium potential for chloride more negative than resting membrane potential. Thus, short-term activation of pyramidal GABA_A receptors produces repolarization or hyperpolarization [42]. In contrast, chloride conductance activation in dorsal root ganglion neurons can yield depolarizing potentials [53]. Developmental changes during the first weeks of life also affect the net result of activating hippocampal chloride channels. GABA_A receptors are excitatory in the neonatal period and become inhibitory with maturation [11]. This transition is related to postnatal upregulation of KCC2 expression [20,46]. While much is known about the functional contribution of ligand-gated chloride channels and chloride transporters to neuronal excitability, little is known about the role of specific CIC chloride channels. A lack of pharmacological agents specific for these channels has compelled the use of a variety of genetic and molecular strategies to study the function of these proteins.

CIC-3 is a member of the CIC family of voltage-gated chloride ion channels. CIC channels play diverse roles in various tissues, including: regulation of muscle excitability and repolarization (CIC-1) [28], cell–cell interactions in the blood–testes and blood–retina barriers (CIC-2) [8], renal proximal tubular endocytosis (CIC-5) [43], and bone metabolism (CIC-7) [29]. CIC-3 is highly expressed in neurons, renal and gastrointestinal epithelial cells [48] and in the media and intima of blood vessels [31]. Within the central nervous system, the highest density of expression is in the hippocampal formation and cerebellum [7,27]. The only member of the CIC family with an identified function in mammalian neurons is CIC-2, which produces an inwardly-rectifying chloride conductance in selected neuronal populations, depending on the state of brain maturation [12,50,53]. Over-expression of CIC-2 in dorsal root ganglion cells resulted in a large negative shift in the Cl^- equilibrium potential that attenuated GABA -mediated membrane depolarization and prevented GABA_A receptor-mediated action potentials. However, CIC-2 ‘knockout’ mice show no alteration in seizure threshold and have a structurally normal central nervous system (CNS), aside from retinal degeneration due to a defect in the retinal blood–tissue barrier [8]. CIC-4 is expressed in hippocampus and cerebellum [1], and lesser amounts of CIC-5 are expressed diffusely in brain [55], but no abnormal CNS phenotype accompanies the ‘knockout’ of either CIC-4 [41] or CIC-5 in mice [43,65].

Very little information regarding CIC-3 has been derived from studies of neuronal function. Most CIC-3 data has been gleaned from artificial expression systems. The subcellular localization and biophysical nature of CIC-3 channels are topics of considerable debate. CIC-3 has been proposed to be a cell surface channel regulated by (1) swelling [19], (2) calcium-calmodulin-dependent protein kinase II (CamKII) [24] or (3) the cystic fibrosis trans-

membrane regulator (CFTR) [38]. Alternatively, CIC-3 has been proposed to function as an intracellular channel that regulates acidification of synaptic vesicles [58] or endosomes [72].

Neuronal excitability could be most directly affected by CIC-3 if the channel is present at the cell surface and active at physiological voltages. What is the evidence that CIC-3 functions in the plasma membrane? When CIC-3 was initially expressed in *Xenopus* oocytes [27] or in Chinese hamster ovary cells (CHO-K1) [34], outwardly-rectifying chloride currents were observed that were blocked by activation of protein kinase C (PKC) [27]. Subsequent expression of cloned CIC-3 in NIH 3T3 fibroblasts resulted in similar outwardly rectifying currents that were activated by cell swelling and inhibited by PKC at a specific site [18]. In contrast, human epithelial cells stably transfected with the full-length human CLCN3 gene displayed a CaMKII-regulated Cl^- current that was not activated by changes in cell volume [24]. Finally, two different groups have demonstrated that at least a proportion of CIC-3 is present in the plasma membrane because CIC-3 protein can be labeled using the membrane-impermeant thiol-reactive reagent, biotin-maleimide [24,66].

The initial report on *Clcn3*^{-/-} gene ‘knockout’ mice demonstrated that lack of the CIC-3 protein in did not eliminate normal volume-regulated chloride conductances in hepatocytes or pancreatic acinar cells. Most strikingly, these mice displayed rapid degeneration of the hippocampus and retina [58]. Electrophysiologic examination of CA1 pyramidal cells in mouse pups prior to neuronal loss revealed no major abnormalities, other than slightly increased glutamate-mediated miniature post-synaptic excitatory potentials, and diminished synaptic plasticity as indicated by decreased post-synaptic potentiation. CIC-3 co-localized with synaptic vesicle proteins isolated from normal mouse brain, and acidification was slowed in *Clcn3*^{-/-} synaptic vesicles. These authors concluded that CIC-3 is an intracellular anion channel involved in the regulation of synaptic vesicular pH, and they hypothesized that neuronal degeneration might be due to excitotoxicity secondary to enhanced glutamate packaging within synaptic vesicles.

A second, independently-generated *Clcn3*^{-/-} mouse was recently reported to display a similar neurodegenerative process, that reportedly resembles human ceroid lipofuscinosis [72]. Subunit c of mitochondrial F1F10 ATPase was shown to have accumulated in lysosomes of the *Clcn3*^{-/-} mouse, and an elevation of hepatic endosomal pH was detected. Localization of CIC-3 to lysosomes has also been demonstrated in a heterologous expression system [35]. However, lipofuscin is not apparent in the electron microscope photographs presented in the study of Stobrawa et al. [58].

Clearly, significant debate remains regarding the regulation and localization of CIC-3 channels in general, and their function in neurons in particular. We also indepen-

dently created a mouse lacking CIC-3, as reported in preliminary form [49]. The major CNS defects (hippocampal degeneration, retinal blindness, behavioral excitability) in our *Clcn3*^{-/-} mice confirm the basic features described by the other groups [58,72].

The objectives of the present study were to: (1) create a *Clcn3*^{-/-} ‘knockout’ mouse model, (2) characterize its phenotype, particularly with regard to the brain and behavior, (3) investigate in detail the time course and anatomical sequence of neurodegeneration and gliosis in the dentate gyrus and hippocampus, and (4) test the hypothesis that hippocampal degeneration is related to recurrent seizures by measuring the susceptibility of the mice to drug-induced seizures. Results of these studies led us to examine GABAergic function more closely. We present pharmacological and immunohistochemical evidence that alterations in GABAergic function precede and accompany hippocampal degeneration. Our data support the hypothesis that lack of a functional CIC-3 chloride channel disturbs the balance of inhibition and excitation within the hippocampus and contributes to neurotoxicity in the *Clcn3*^{-/-} mouse.

2. Materials and methods

2.1. Construction of replacement vector and gene targeting

A *Clcn3* replacement vector, pBYC1c3, was constructed in two cloning steps. For the 3' homology, a 3.6 kb Bgl II fragment, including part of intron 7, exons 8 and 9, and part of intron 9, was subcloned into the BamHI site of pOSdupdel (a gift of O. Smithies, University of North Carolina at Chapel Hill, NC, USA). The BclI site located within intron 7 was removed by digestion with *BclI* and Klenow filling-in. For the 5' homology, a 2.1 kb polymerase chain reaction (PCR) fragment, containing part of intron 5 and part of exon 6, was subcloned into the BclI and XhoI sites of pOSdupdel. This targeting vector deletes part of transmembrane domain 2, located in exon 6, and all of transmembrane domains 3 and 4, located in exon 7. The targeting construct was linearized and introduced into R1 embryonic (ES) cells (129X1/SvJ×129S1/Sv) via electroporation. The ES cells were then cultured for 24 h in regular medium [DMEM-H+15% fetal calf serum (FCS)] and 10 to 14 days in selection medium (regular medium+G418 at 200 µg/ml+gancyclovir at 2 µM). Surviving colonies were picked and expanded for screening. The colonies were analyzed by Southern blot analysis using *NdeI* restriction digestion and hybridization with a 1 kb PCR product amplified from intron 9. Of the 69 colonies picked, two showed the distinct targeted allele and were used for generation of chimeras via blastocyst microinjection.

2.2. Generation of *Clcn3*^{-/-} mice

The parental ES cell line R1 was derived from mouse strain 129/SvJ, which carries an Agouti (A^w) coat color marker. ES cells heterozygous for the mutant *Clcn3* alleles were injected into C57Bl/6J blastocysts. Chimeric animals were bred and the DNA of their progeny assayed for presence of the mutant allele. Both lines (derived from the two colonies isolated above) of chimeras transmitted the ES cell genome to the next generation when chimeric males were bred to C57Bl/6J females. Heterozygous F1 hybrids were intercrossed to generate homozygotes. Thus, the genetic background of animals used in this study is a mixture of 129/Sv and C57Bl/6J.

Progeny were genotyped using PCRs. Primers specific for the wild type allele were derived from exon 7 and intron 7 (forward, 5'-TACATGTTGCCTGCTGCTGT-3'; reverse, 5'-CTGCAGCACTCAACTCCAGA-3') and primers specific for the knockout allele were derived from the neomycin gene (forward, 5'-TGAATGAACTGCAGGACGAG-3'; reverse, 5'-ATACTTTCTCGGCAGGAGCA-3'). PCRs contained 1 µl of cDNA or 40 ng of total mouse DNA added to 0.25 U BIO-X-ACT DNA polymerase (Bioline, Kenilworth, NJ, USA) in the buffer with 1.5 mM MgCl₂, 200 µM dNTPs, and 1 µM primers. Conditions for the PCR experiments were: 94 °C denaturation for 2 min, 57 °C annealing for 30 s, 68 °C extension for 1 min, 35 cycles.

2.3. Western blot of CLC-3 protein

Mouse brain homogenates were used to identify native CIC-3 protein. Tissues were prepared as previously described [62]. Mouse brains were homogenized twice by 10-s strokes at power level 5 with a Polytron homogenizer (Brinkmann Instruments, Westbury, NY, USA) in 5 ml/g tissue of homogenization solution [10 mM HEPES adjusted to pH 7.4 with Tris, 10% sucrose, 1 mM EDTA, 1 mM phenylmethylsulfonyl fluoride (PMSF), with one tablet of COMPLETE protease inhibitor (Roche Applied Science, Indianapolis, IN, USA) per 50 ml]. Homogenates were centrifuged at 2,500 g for 15 min at 4 °C and the supernatants were saved. The pellets were resuspended in 5 ml of homogenization buffer per gram of starting tissue, then homogenized and recentrifuged as above. The supernatants were combined and crude membrane proteins were precipitated by centrifugation at 22,000 g for 20 min at 4 °C. The supernatants from this step were discarded and the pellets were resuspended in phosphate-buffered saline (PBS) containing 1 mM EDTA, 1 mM PMSF, and ‘COMPLETE’ protease inhibitor (one tablet per 50 ml) then passed once through a 25-gauge needle and once through a 30-gauge needle. Aliquots were quickly frozen in liquid N₂ and stored at -85 °C until use.

Approximately 100 µg of crude membrane protein was separated by two-phase Tricine-polyacrylamide gel elec-

trophoresis (10% T/6% C resolving layer, 4% T/3% C stacking layer), and transferred onto nitrocellulose membrane (Hybond ECL, Amersham Pharmacia Biotech, Piscataway, NJ, USA) in buffer containing: 10 mM CAPS adjusted to pH 11 and 10% methanol. The blot was blocked overnight at room temperature in blocking buffer [PBS containing 1% Tween-20, 4% bovine serum albumin (BSA), and 1% normal goat serum]. After blocking, the blot was incubated for 2 h at room temperature in blocking buffer containing a 1:250 dilution of rabbit anti-CIC3 polyclonal antibody (Alomone Laboratories, Jerusalem, Israel), washed 3× with PBS-T (PBS containing 1% Tween-20), incubated for 1 h at room temperature in blocking buffer containing a 1:5000 dilution of horseradish peroxidase (HRP)-conjugated goat anti-rabbit IgG (Jackson ImmunoResearch Laboratories, West Grove, PA, USA), and again washed 3× with PBS-T. Immune complexes were detected on film using Enhanced ChemiLuminescence (Amersham Pharmacia Biotech).

2.4. Mouse phenotyping: growth, survival, general appearance, and behavior

All mice were fed standard mouse chow and water, ad libitum, and maintained on a 12:12 h light:dark schedule. Care of mice in these experiments met or exceeded standards set forth by the National Institutes of Health in their guidelines for care and use of experimental animals. All procedures were approved by the University of Iowa Animal Care and Use Committee.

Mice were weighed at the time of tail tissue collection for genotyping, at weaning and periodically thereafter. The mouse colony was checked for animal deaths daily and fully inventoried at least once each month in order to assess survival of the different groups of mice. General and specific behaviors of the mice were observed. The escape extension response to tail elevation was evaluated by measuring the time to onset of rear-leg folding in unsexed mice held by the tail, 30 cm above a flat surface for 1 min.

Blood tests were performed for pH, electrolytes, Ca^{2+} , Mg^{2+} , and glucose metabolism, to assess for abnormalities that could affect neuronal function. Blood gas measurements were performed using an IL 1620 blood gas analyzer (Instrumentation Laboratories, Lexington, MA, USA) on venous retro-orbital blood samples drawn with capillary tubes from sedated mice (midazolam HCl, Roche, 10 mg/kg s.c.). Hematocrits were measured from separate retro-orbital blood samples in 70 μl capillary tubes that were permitted to stand vertically for 1 h before being spun (5 min) in a capillary microcentrifuge. Serum chemistry tests were performed by the University of Iowa Clinical Laboratories.

For glucose tolerance tests, mice were fasted overnight but permitted access to water. A dose of 2 g glucose/kg (200 μl /20 g of body weight of a 20% glucose solution)

was administered intraperitoneally to unsexed mice. Blood samples were taken from a nick in the tail vein and drawn by capillary action into microcuvettes (B-glucose HemoCue Microcuvettes, Angelholm, Sweden), and placed into a B-Glucose Analyzer (HemoCue). Time points for measurement included: baseline, 30, 60, 90, and 120 min. To minimize total blood volume taken from each mouse, a separate group of mice was fasted overnight and serum insulin levels were measured using an enzyme-linked immunosorbent assay (ELISA) kit (#90060, Crystal Chem Inc., Chicago, IL, USA).

To quantify spinal conformation and assess kyphosis, mice were sedated with midazolam HCl, (10 mg/kg s.c., Roche) and suspended by the tail in front of an X-ray film cassette for both lateral and frontal position X-rays of skeletal structure. The force applied to straighten the spine therefore consisted of the body weight of each individual mouse. This sedated, suspension method controlled for variations in muscle tone and avoided artifactual curvatures associated with positioning of an unconscious mouse. Thoraco–lumbar and cervico–thoracic angles were measured with a protractor from lateral view X-rays. Knockouts were gender-matched to heterozygote littermates, and when an appropriate littermate was not available, an age and gender-matched control was used.

2.5. Histology

For neuropathological studies, wild type, heterozygous and knockout mice were sacrificed at a series of ages ranging from postnatal day (PD) 23 to PD678. Three animals of each genotype were included for each age range. Following a lethal injection of pentobarbital (>50 mg/kg, i.p., to effect), the mice were perfused via the left ventricle with ice cold 0.1 M phosphate buffer, followed by a fixative containing 4% paraformaldehyde in 0.1 M phosphate buffer. The brains were removed and stored in cold fixative for a minimum of 1 week. Some of the brains were dehydrated through a graded series of alcohol, prior to paraffin embedment. The paraffin-embedded tissue was cut on a rotary microtome in the coronal plane at a thickness of 5 μm . Sections throughout the rostral–caudal axis of the brain were mounted onto glass slides and a 1:4 series of sections was Nissl-stained with cresyl violet. The remaining fixed brains were placed in 30% sucrose in 0.1 M sodium phosphate until they sank. Forty-micrometer-thick frozen sections were cut horizontally on a sliding microtome and either Nissl-stained or used for immunostaining.

To determine whether the neuronal loss observed in the knockout mice was accompanied by astrogliosis, sections were stained immunohistochemically for glial fibrillary acidic protein (GFAP), a specific marker for astrocytes within the CNS. These sections were first incubated with 3% hydrogen peroxide for 30 min, followed by goat serum blocking solution for 60 min, then incubated with a

monoclonal guinea pig anti-mouse GFAP antibody (Sigma, St. Louis, MO, USA). Detection was performed using biotinylated goat anti-guinea pig secondary antibody (Vector Laboratories, Burlingame, CA, USA), followed by ABC Elite (Vector) and diaminobenzidine (Vector). PBS was used for all dilutions and rinses.

In addition to GFAP, brain sections from animals at PD23 and PD73 were stained immunohistochemically for glutamic acid decarboxylase (GAD-67), the enzyme responsible for the synthesis of GABA, or for the GABA_A receptor. The immunohistochemical technique for the GAD-67 and GABA_A receptor staining was identical to that used for GFAP staining except that the secondary antibodies were produced in horses, so that the blocking solution employed was horse serum. The primary antibodies were goat anti-mouse GAD-67 (catalog No. SC-7512) and goat anti-mouse GABA_A R alpha5 (catalog No. sc-7356) obtained from Santa Cruz Biotechnology (Santa Cruz, CA, USA). The secondary antibody was horse anti-goat IgG (Vector Laboratories, catalog No. BA9500). For the diaminobenzidine reaction, all sections were allowed to react for 7 min.

GAD-67 and GABA_A receptor immunolabeling was quantitatively assessed through the use of an image analysis system. Single representative horizontal sections at the level of the mid septo-temporal hippocampus were analyzed for each mouse ($n=3$ wild type, heterozygote, and knockout at each of two ages, PD23 and PD73, for a total n of 18 for both GAD-67 and GABA_A receptor). In each analyzed section, the hippocampal formation was digitally photographed utilizing uniform levels of contrast and brightness, generating an eight-bit gray-scale image.

The relative densities of GABA_A receptor and GAD-67 immunolabeling in hippocampal stratum granulosum and stratum pyramidale of CA3 and CA1 were measured through the use of the NIH public domain Image J image analysis software. For both GABA_A receptor and GAD-67, regions of lightly-stained and of darkly-stained tissue were first identified among the entire set of analyzed images, and the density of pixels within those regions were measured. A linear calibration function was then established by assigning a gray value of 1 to the pixel value of the lightly stained region and a gray value of 100 to the pixel value of the darkly stained region.

For each of the analyzed sections, stratum granulosum of the dentate gyrus, and stratum pyramidale of the CA3 and CA1 regions of the hippocampus were traced, and the mean gray values within those regions were determined by the Image J software. In order to account for possible differences in background levels of staining in each section, mean gray values were also determined over regions of white matter within the same tissue sections. The density of staining at each of the analyzed regions was expressed as the ratio of mean gray value within each hippocampal region to mean gray value of background.

For studies of eye and muscle histology, tissues were

obtained from the same deeply anesthetized, perfused animals as above. Tissues were dissected postmortem and examined at the macroscopic level before additional fixation in 4% paraformaldehyde in PBS. Fixed tissue was embedded in paraffin, sectioned (8 μ m), stained by hematoxylin and eosin (H&E) according to standard protocols and examined by light microscopy.

2.6. Behavioral responses to drugs

Drug experiments were conducted in a quiet daytime laboratory setting, and behavioral responses were assessed in terms of type, time of onset, duration, severity, and lethality (if any). There was a minimum 1-week washout period after midazolam before any other studies were conducted. Midazolam (10 mg/kg i.p.) was administered to mice aged 3–4 months which were observed for up to 2 h, or until the mouse recovered and was ambulating spontaneously and with normal locomotion. Because of the loss of the righting reflex in the *Cln3*^{-/-} mice, and the association of this behavior with anesthetic indices, reflex withdrawal responses were assessed every 10 min in all mice by light toe pinch using forceps.

The pro-convulsant, pentylenetetrazole (PTZ), was dissolved at 7 mg/ml in sterile 0.9% NaCl and administered to 4–5-week-old mice (70 mg/kg i.p.). To determine whether resistance to PTZ-seizure induction persisted into adulthood, the drug was given to a separate group of mice aged 3–4 months (52.5 mg/kg i.p.). The lower dose of PTZ was selected for the adult mice because 70 mg/kg i.p. proved lethal to adult mice of all three genotypes, and the dose of 35 mg/kg was not consistently effective in producing seizure activity in the control mice. Parameters measured during the 60-min observation period included time to onset of behavioral arrest, myoclonic jerks, generalized tonic-clonic seizures or full tonic extension, and duration of the first generalized seizure, if one occurred. Lethality was assessed 60 min post-injection [36].

Kainic acid (KA, 30 mg/kg i.p) was administered to 4–6-week-old mice. The dose of KA was selected based on dose–response studies conducted in the C57/black strain of mice [23]. Seizure-related and complex stereotypical activity was observed for up to 2 h. KA-induced seizure related behaviors were graded using a scale derived from those of Levkovitz et al. [32] and Hu et al. [23]. We defined KA-induced seizure activity as follows: grade 1: behavioral arrest, staring; grade 2: myoclonic jerks of limbs, head, neck, or thorax, or head nodding/swaying; grade 3: unilateral clonic activity, front or hindlimb pawing, may result in circling; grade 4: bilateral forelimb tonic or clonic activity (pawing the air, rearing, jumping, wobbling, falling); grade 5: generalized tonic/clonic activity with loss of postural tone, with or without death. We measured the latency to onset of the first occurrence of each grade of seizure-related activity. The

durations of generalized seizures were noted, where practical, but in most cases individual behavioral abnormalities, once expressed, recurred over extended periods (1–2 h). We did not use this scale for PTZ-induced seizures because PTZ has qualitatively different effects, and only grades 1, 2 and 5 would apply.

To avoid any kindling effects, each mouse was tested with only one of the two seizure-inducing drugs, in a single experiment. To avoid confounding the data in other projects, mice that had received either KA or PTZ were excluded from all subsequent behavioral tests and from brain histologic analysis.

2.7. Statistical analysis

Unless otherwise stated, numbers of males and females were balanced within each genotype, and animals were age-matched as closely as possible when a littermate was not available. Comparisons between groups of animals were performed by one-way analysis of variance (ANOVA). Dunnett's test for multiple comparisons (seizure data) or Newman–Keuls post-hoc analysis (immunostaining) were employed when the F statistic of the ANOVA was significant ($P < 0.05$). t -Tests were used when only two groups were compared. The Wilcoxon rank sum test

was used for non-parametric comparisons. When only two groups (i.e., males versus females) were compared non-parametrically, the proportions of mice in each group exhibiting a characteristic (e.g., survival to a time point) were compared using z -tests. The numbers of mice born with each genotype were compared to the expected Mendelian ratios using the Chi-square test. $P < 0.05$ was interpreted as statistically significant. Values were expressed as the mean \pm S.E.M.

3. Results

3.1. Disruption of the *Clcn3* gene and generation of *Clcn3*^{-/-} mice

A null mutation in the *Clcn3* gene was generated by replacing part of exon 6 and all of exon 7 with a cassette containing the neomycin resistance gene (Fig. 1A). Appropriate gene targeting was detected by Southern blot analysis (Fig. 1B) in two of 69 colonies surviving double selection. Both lines of chimeras transmitted the ES cell genome to the next generation when bred to C57BL/6J females. Heterozygous F1 hybrids from chimera breeding were intercrossed to generate homozygotes. The knockout

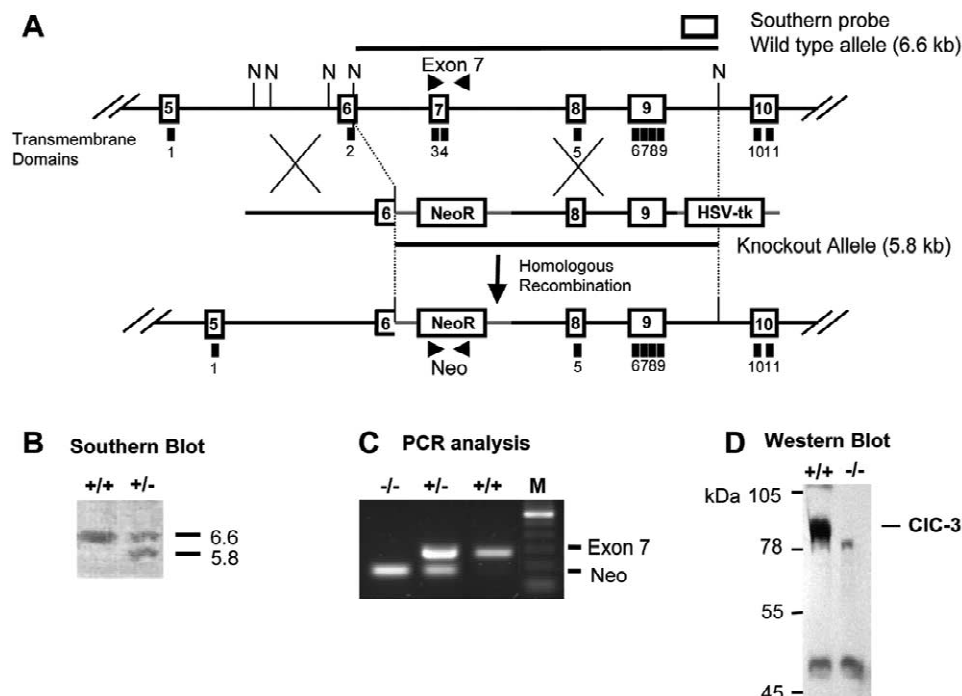


Fig. 1. Targeted inactivation of the *Clcn3* gene. (A) The structure of the *Clcn3* gene for exons 5 through 10, the replacement vector and the targeted allele. The knockout allele replaces 13 bp of exon 6 and all of exon 7 with vector sequence including the neomycin resistance gene (NeoR). (B) Embryonic stem cells were genotyped by Southern blot analysis. When genomic DNA was digested with the restriction enzyme *NheI* (N), the probe (open rectangle at top) detected a 6.6 kb fragment representing the wild type allele and a 5.8 kb fragment for the knockout allele. (C) Genotyping of mice by PCR. Mice homozygous for the knockout allele (-/-), heterozygous (+/-) and homozygous for the wild type (+/+) were identified by PCR amplified from mouse genomic DNA using primers specific for the wild type *Clcn3* gene (exon 7) and the neomycin resistance gene (Neo), respectively. A 100 bp ladder is included as a size standard (M). (D) Western blot analysis shows that the CIC-3 protein is present in mice that are homozygous for the wild type (+/+) allele and absent in mice that are homozygous for the knockout (-/-) allele. Migration of molecular weight standards (kDa) is indicated at left.

and wild type alleles were detected by PCR using primers specific for the neomycin resistance gene and exon 7, respectively (Fig. 1C). Western blotting of brain membrane proteins revealed a complete absence of CIC-3 protein in the *Clcn3*^{-/-} mouse (Fig. 1D).

When 578 intercross progeny from 79 litters were genotyped, the ratio of *Clcn3*^{+/+}, *Clcn3*^{+/-} and *Clcn3*^{-/-} mice (127, 330, 121) resulting from *Clcn3*^{+/-} × *Clcn3*^{+/-} breedings was not statistically different than expected from predicted Mendelian ratios, demonstrating that the *Clcn3* gene is not required for viability at birth. Some, but not all, male *Clcn3*^{-/-} mice successfully fathered litters that contained normal numbers of healthy pups. Only one litter was ever observed from numerous pairings of *Clcn3*^{-/-} females and *Clcn3*^{+/-} males. That litter of four pups died shortly after birth.

3.2. General appearance, growth, survival, and behavior

Both the growth and survival of *Clcn3*^{-/-} mice were impaired substantially compared to age- and gender-matched *Clcn3*^{+/-} and *Clcn3*^{+/+} mice (Fig. 2). There were no major differences in the growth (Fig. 2A, B) or survival for *Clcn3*^{+/-} mice compared to *Clcn3*^{+/+} mice (survival data for wild types not shown). Male and female *Clcn3*^{+/-} and *Clcn3*^{+/+} mice continued to gain weight throughout the first 6 months of life. Adult male *Clcn3*^{-/-} mice rarely exceeded 30 g (Fig. 2A), and female *Clcn3*^{-/-} mice rarely exceeded 25 g (Fig. 2B). The weight difference between *Clcn3*^{-/-} mice and their littermates was significant as early as PD9–PD11 for both males: knockouts 4.5 ± 0.2 g, (n=23); heterozygotes 6.7 ± 0.3 g, (n=25); wild type 6.1 ± 0.2 g, (n=25) and females: knockouts

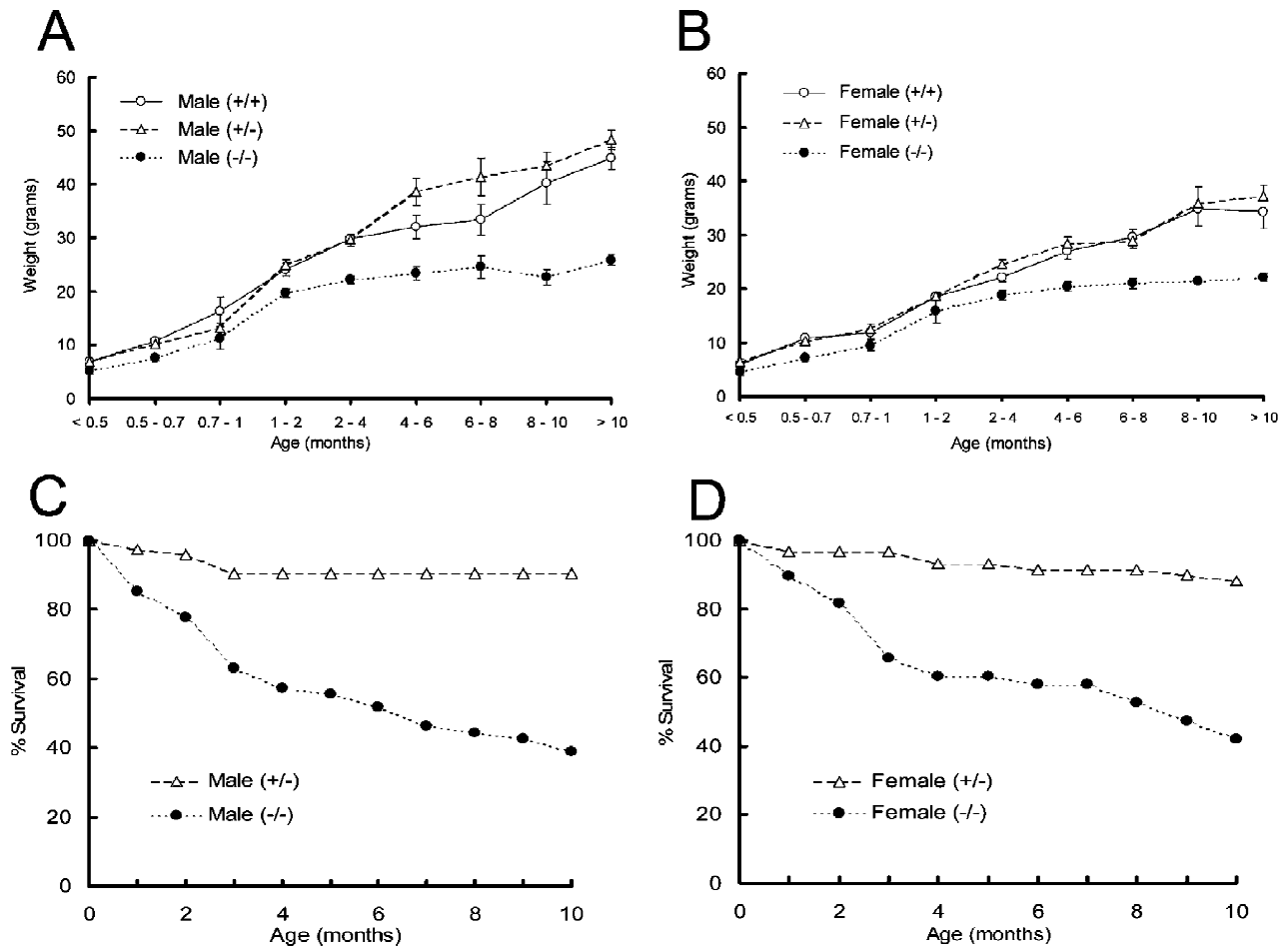


Fig. 2. Growth and survival of *Clcn3*^{-/-} mice. At all time points from 1 month and onwards in panels A–D, *Clcn3*^{-/-} mice show statistically significant differences from their gender-matched littermates. (A) Growth of male *Clcn3*^{-/-} mice is less than that of male *Clcn3*^{+/-} and *Clcn3*^{+/+} mice. (B) Similarly, growth of female *Clcn3*^{-/-} mice is impaired compared to female *Clcn3*^{+/-} and *Clcn3*^{+/+} mice. (C) Survival curves indicate high mortality rate in the first 10 months of life in male *Clcn3*^{-/-} mice compared to male *Clcn3*^{+/-} mice. Survival of *Clcn3*^{+/-} mice was not different from that of *Clcn3*^{+/+} mice (data not shown). (D) Survival curves demonstrate that female *Clcn3*^{-/-} mice have greater mortality than female *Clcn3*^{+/-} mice. Comparison with (C) shows there are no differences in mortality rates between male and female *Clcn3*^{-/-} mice at any time point in the first 10 months of life.

4.5±0.3 g ($n=22$); heterozygotes 6.2±0.4 g ($n=23$); wild type 5.9±0.3 g ($n=23$).

Knockout mice died prematurely and unexpectedly (Fig. 2C, D), without any obvious prodrome of illness. The death rate was fairly constant throughout the first 10 months of life, with the exception of a peak in deaths associated with weaning, and otherwise was not increased significantly during the first 2 months of life when rapid degenerative changes were occurring in the hippocampus and retina. By 3 months, one-third of all knockout mice had died, and by 6 months half were dead. No gender-related differences in survival were seen at any time point during the first 10 months of life. Post-mortem exams did not reveal any obvious pathology that could account for cause of death. However, one striking post-mortem feature was a relative absence of fat in the abdominal and other body cavities in adult *Clcn3*^{-/-} mice compared to similar-aged *Clcn3*^{+/-} and *Clcn3*^{+/+} mice. In mice aged 5–10 months, femur lengths were not statistically different among male *Clcn3*^{+/-} mice (15.8±0.26 mm, $n=13$), male *Clcn3*^{-/-} mice (15.6±0.21 mm, $n=9$), female *Clcn3*^{+/-} mice (15.9±0.14 mm, $n=12$) and female *Clcn3*^{-/-} mice (16.2±0.82 mm, $n=3$). If femur length is taken as a proxy for overall skeletal size, these data support the conclusion that the weight differences between *Clcn3*^{-/-} and *Clcn3*^{+/-} mice are due to differences in soft tissue mass (including fat) rather than differences in overall development of the skeleton.

We performed a series of general screening blood tests (Table 1) in order to detect any gross abnormalities in major organ function that could affect survival, brain function, arousal, or excitability. No significant differences

in serum Na, Cl, HCO₃, pH, Ca, Mg, osmolality or hematocrit were detected between *Clcn3*^{-/-}, *Clcn3*^{+/-} and *Clcn3*^{+/+} mice. *Clcn3*^{-/-} mice showed no significant elevation of creatine kinase, a non-specific indicator of muscle damage. Glucose tolerance tests (Table 1) were performed on fasting *Clcn3*^{+/-}, *Clcn3*^{+/+} and *Clcn3*^{-/-} mice challenged with a glucose load. Fasting blood glucose was significantly lower in *Clcn3*^{-/-} mice (132±7 mg/dl, $n=6$, $P<0.05$) than in the other two groups (*Clcn3*^{+/-}, 170±13 mg/dl, $n=6$; *Clcn3*^{+/+}, 170±13 mg/dl, $n=6$). The *Clcn3*^{-/-} animals also had a lower peak glucose (212±8 mg/dl, $P<0.05$) compared to either control group (*Clcn3*^{+/-}, 358±48 mg/dl; *Clcn3*^{+/+}, 364±54 mg/dl), after being challenged with an intra-peritoneal glucose load. These results are not consistent with an abnormality of either insulin secretion or cellular uptake of glucose. To further confirm this point, fasting insulin levels were measured from a separate group of mice, and there was no significant difference between *Clcn3*^{+/+} and *Clcn3*^{-/-} mice (*Clcn3*^{+/+}, 1.27±0.38 ng/ml, $n=6$; *Clcn3*^{-/-}, 0.67±0.46 ng/ml, $n=5$).

In general, *Clcn3*^{-/-} mice were ‘jittery’ and excitable, and walked with a slightly waddling gait. These abnormalities were observed at very early ages (2–3 weeks), prior to the onset of histologically evident hippocampal and retinal degeneration. We observed that adult *Clcn3*^{-/-} mice exhibited a prolonged recovery time from benzodiazepines and barbiturates during preparation for noninvasive studies (midazolam) or surgical instrumentation (pentobarbital). Pentobarbital doses (20–25 mg/kg, i.p.) approximately half of normal were sufficient to induce a surgical plane of anesthesia, but often produced death in

Table 1
Blood tests in *Clcn3*^{+/-}, and *Clcn3*^{+/+} mice

	(+/+)	<i>n</i>	(+/-)	<i>n</i>	(-/-)	<i>n</i>
Electrolytes						
Sodium (mequiv./l)	151±3.6	6	152±2.2	10	149±3.0	10
Chloride (mequiv./l)	114±1.8	5	119±3.1	7	119±4.2	6
Calcium (mg/dl)	8.4±0.4	6	9.5±0.68	7	9.8±0.17*	5
Albumin (g/dl)	2.7±0.3	5	2.9±0.4	5	3.0±0.2	5
Magnesium (mg/dl)	2.3±0.3	5	3.4±0.55	5	2.62±0.10	5
Blood gases						
pH	7.22±0.02	8	7.23±0.03	9	7.23±0.02	8
pCO ₂ (Torr)	47.3±3.1	8	45.5±4.0	9	46.8±3.5	8
HCO ₃ (mequiv./l)	19.8±1.6	8	19.7±2.2	9	20.0±1.5	8
Glucose tolerance						
Fasting (mg/dl)	170±13	6	170±13	6	132±7.0*	6
30 min	342±35	6	344±55	6	208±11* #	6
60 min	309±60	6	327±49	6	179±11* #	6
90 min	267±63	6	292±37	6	171 + 7.0 #	6
120 min	235±56	6	240±24	6	147±10 #	6
Hematocrit						
	54.3±1.4	20	56.0±2.3	8	56.5±2.9	8

* Indicates $P<0.05$ comparing (+/+) to (-/-).

Indicates $P<0.05$ comparing (+/-) to (-/-).

Clcn3^{-/-} mice, compared to the well-tolerated effects of the usual dose (50 mg/kg, i.p.) in *Clcn3*^{+/-} or *Clcn3*^{+/+} mice.

As part of a screen for abnormal vestibulocerebellar function [30,60] or altered neuromuscular function [13], we examined responses to tail elevation. When the tail is elevated in conscious mice, the normal response (Fig. 3A) is to splay the limbs (especially the hindlimbs) in a behavior termed ‘escape extension’ [33]. When mice were suspended by the tail, an abnormal rear leg-folding behavior (Fig. 3B) was exhibited within 30 s by 10 of 15 (66.7%) of knockouts, 1 of 17 (3.9%) heterozygotes, and 0 of 9 wild types. Within 1 min 12 of 15 (80%) knockout mice exhibited this behavior, and there was no change in the response rate for *Clcn3*^{+/-} or *Clcn3*^{+/+} mice (Fig. 3D). At both 30 and 60 s, the proportion of knockouts exhibiting this hindlimb behavior was statistically greater than in the control groups ($P<0.05$). The forelimb response to tail suspension of *Clcn3*^{-/-} mice was not consistent within the group, nor within a given mouse at different times. *Clcn3*^{+/+} and *Clcn3*^{+/-} mice usually reached outward and forward with the forelimbs (Fig. 3A). In addition, 2 of 15 (13%) knockout mice drew in both hindlimbs and forelimbs and flexed the body into a fetal position (Fig. 3C, D), such that the nose pointed upwards.

Gross physical observation of the *Clcn3*^{-/-} mice showed a markedly kyphotic spine. We wished to determine whether this arched posture [58] of *Clcn3*^{-/-} mice was in fact a behavioral feature or an anatomic musculoskeletal characteristic. In sedated mice, lateral plane X-rays (Fig. 4A) revealed that both the thoracolumbar [*Clcn3*^{-/-}; $140\pm 3.3^\circ$ ($n=12$), *Clcn3*^{+/-}; $156\pm 1.9^\circ$ ($n=13$), $P<0.05$] and cervicothoracic (*Clcn3*^{-/-}; $125\pm 3.4^\circ$, *Clcn3*^{+/-}; $135\pm 1.7^\circ$, $P<0.05$) angles were

significantly different compared to age- and gender-matched controls. *Clcn3*^{+/-} and *Clcn3*^{-/-} mice selected for Fig. 4A and B, respectively, represented individuals with anterior–posterior curvatures close to their group averages, whereas Fig. 4C shows an example of a *Clcn3*^{-/-} mouse with more severe spinal curvature. Comparable measurements were made on frontal plane X-rays to assess the presence of scoliosis, but yielded no differences among groups. General observation indicated no gross differences in spine conformation between *Clcn3*^{+/-} and *Clcn3*^{+/+} mice.

Because of the kyphosis described above, and because absence of escape extension (especially in hindlimbs) can suggest the presence of a myopathy [13], we examined diaphragm and skeletal muscle tissues to determine if kyphosis was secondary to muscular dysplasia or dystrophy. Hindlimb skeletal muscle samples from nine *Clcn3*^{-/-} mice, seven *Clcn3*^{+/-}, and five *Clcn3*^{+/+} mice were fixed, sectioned, stained with H&E, and examined with light microscopy by a pathologist experienced in detecting myopathies in other transgenic lines of mice. Nine hindlimb specimens were from weanling mice (age 22–33 days), seven from young adults (53–126 days), and five from aged adults (316–556 days). Diaphragm muscle was examined in seven of these mice. No evidence of myopathic changes was seen (data not shown). As a further screen for myopathic processes, serum creatine kinase levels were not different between *Clcn3*^{-/-} (284 ± 81 , $n=11$) and *Clcn3*^{+/-} (353 ± 55 , $n=11$) mice.

We examined H&E stained sections of eyes from five *Clcn3*^{-/-}, four *Clcn3*^{+/-}, and four *Clcn3*^{+/+} mice. In *Clcn3*^{-/-} mice there was a rapid, progressive postnatal degeneration of the retinal photoreceptors, culminating in complete loss of the photoreceptor layer by PD23, as

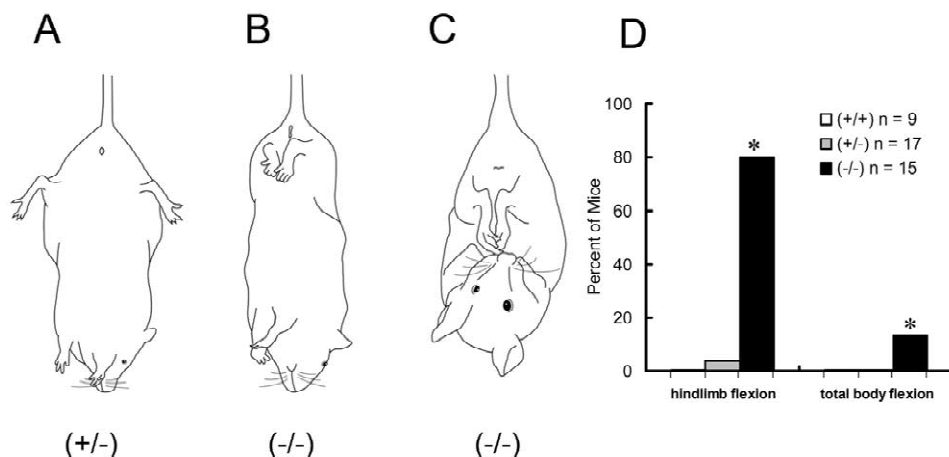


Fig. 3. An abnormal hindlimb grasp is observed in *Clcn3*^{-/-} mice, representing the absence of the escape extension response displayed upon tail elevation in normal mice. (A) Normal response seen in both wild type and heterozygote mice shows normal splaying of the hindlimbs when suspended by the tail. (B) Knockout mouse folds its hindlimbs towards the midline of the body when suspended by the tail. Most *Clcn3*^{-/-} mice display this pattern of abnormal rear leg-folding behavior. (C) Upon tail suspension, a few knockout mice not only fold their rear legs but also their forelimbs, so that the entire body flexes into a ‘fetal’ position. (D) Frequency of hindlimb flexion and total body flexion. Line drawings of mice were derived from photographs (Medical Illustration Department, University of Iowa).

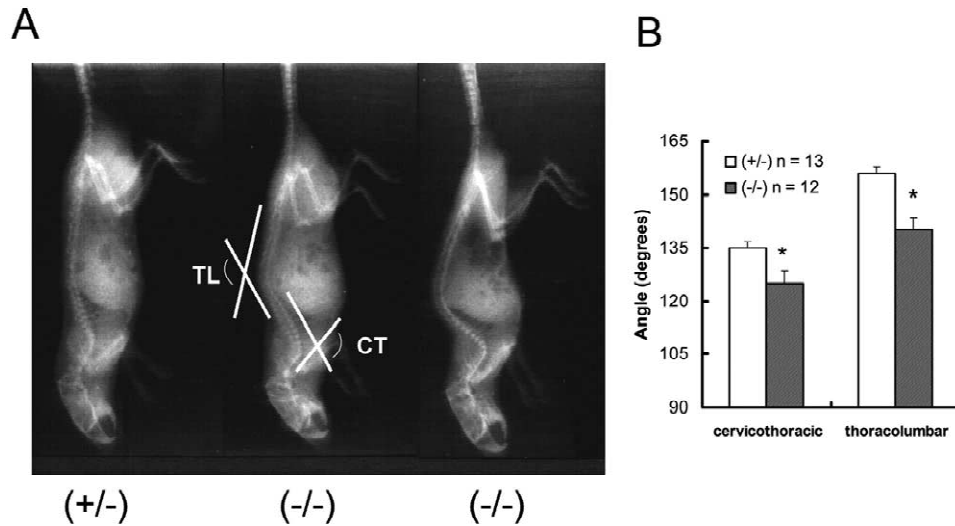


Fig. 4. Lateral view X-rays, illustrating kyphosis in *Clcn3*^{-/-} mice compared to controls. These data show that the hunched posture of *Clcn3*^{-/-} mice is not due to a habitual behavior, but represents a characteristic structural feature of these mice. (A) Left panel: *Clcn3*^{+/-} mouse shows normal spine configuration. Center panel: *Clcn3*^{-/-} mouse exhibiting the abnormal curvatures of thoracolumbar and cervicothoracic spine typically seen in this group. Right panel: more severely affected *Clcn3*^{-/-} mouse, shown at slightly larger scale than center and left panels. Comparison of cervicothoracic and thoracolumbar angles between *Clcn3*^{+/-} and *Clcn3*^{-/-} mice.

shown in Fig. 5. Retinas from heterozygous mice were histologically normal at all ages investigated. Details of the postnatal time course of anatomical and functional retinal degeneration were similar to those described previously [58].

3.3. Central nervous system histology

Clcn3^{-/-} mice exhibited a profound postnatal loss of neurons from the hippocampal formation. This loss of hippocampal neurons was progressive, with a time course

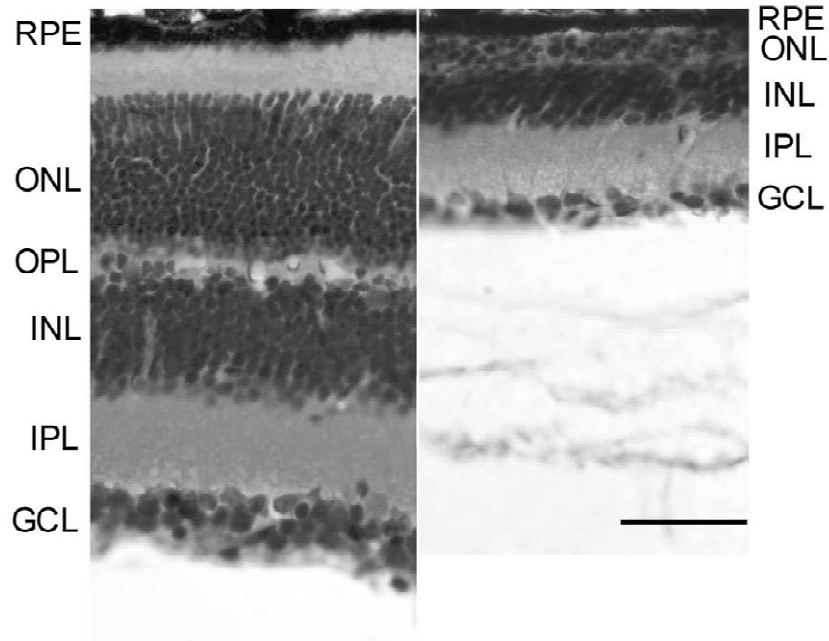


Fig. 5. Retinal degeneration explains the functional blindness observed in *Clcn3*^{-/-} mice. (A) Cross-section of normal retina from a 23-day-old *Clcn3*^{+/+} mouse. RPE, Retinal pigmented epithelium. ONL, Outer nuclear layer. OPL, Outer plexiform layer. INL, Inner nuclear layer. IPL, Inner plexiform layer. GCL, Ganglion cell layer. (B) Retina from a 23-day-old *Clcn3*^{-/-} mouse (littermate of mouse shown in part A) showing marked degeneration and greatly reduced numbers of cells in the photoreceptor layer (ONL), with complete absence of the outer segments. There are greatly reduced numbers of cells in other layers. No retinal abnormalities were observed in *Clcn3*^{+/-} mice. (H&E, calibration bar 50 μ m).

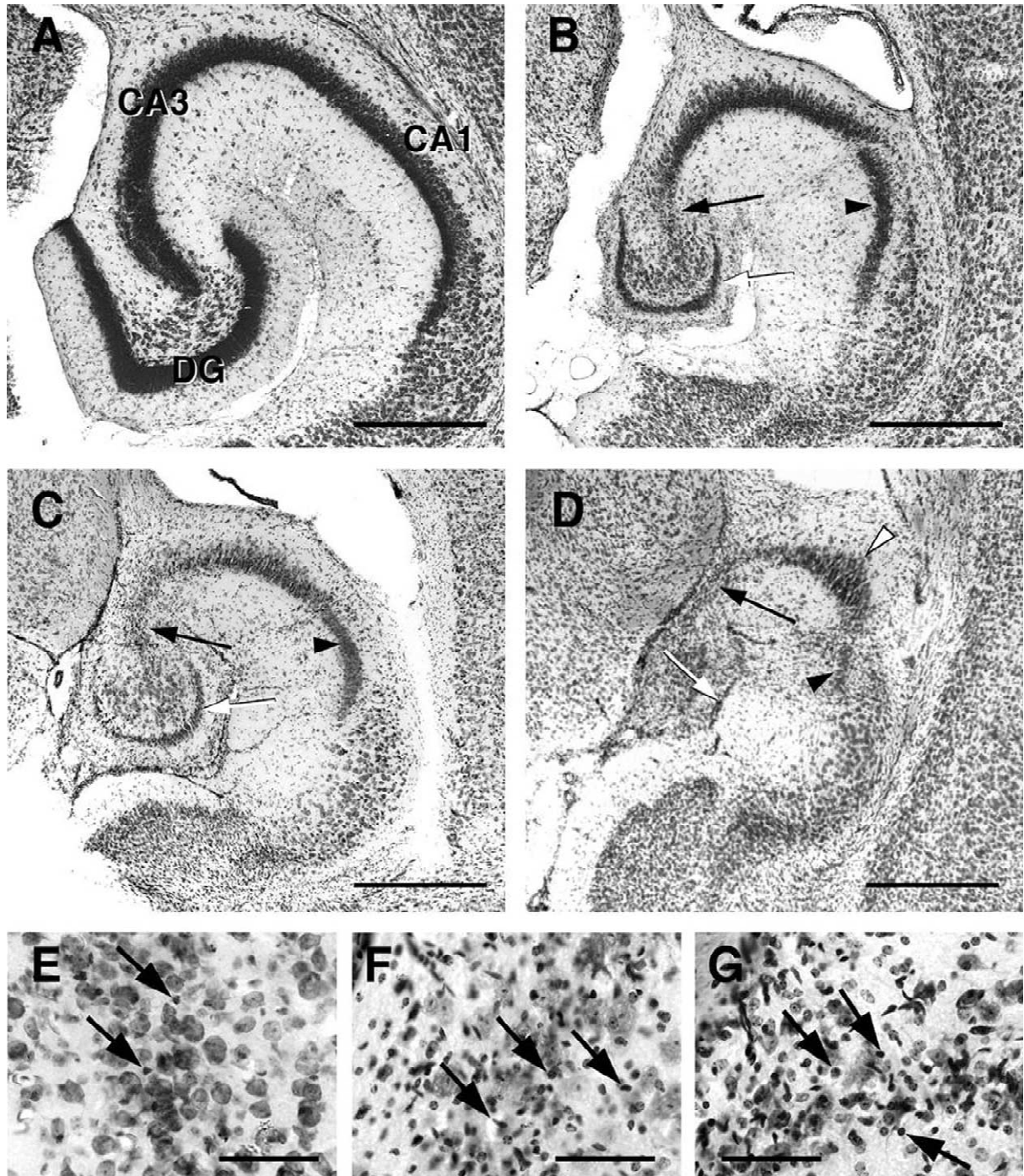


Fig. 6. Nissl-stained horizontal sections taken at the mid-temporal level demonstrate progressive neuronal loss (A–D) and gliosis (E–G) within the hippocampal formation of *Cln3*^{-/-} mice. (A) On PD23, the hippocampal formation appears normal. A full complement of granule cells and pyramidal cells has been generated. The cells have a normal cytoarchitectural arrangement, and no evident loss of neurons has yet occurred. The dentate gyrus (DG), CA3 pyramidal cells, and CA1 pyramidal cells are labeled. (B) By PD75 (2.5 months), there is an evident reduction in the size of the hippocampal formation. In particular, there is a substantial loss of granule cells from the dentate gyrus (white arrow). Near the hilus, there has been some dropout of CA3 pyramidal cells (black arrow). However, the majority of pyramidal cells in both CA3 and CA1 (arrowhead) remain alive at this time point. (C) By PD165 (5.5 months), loss of dentate granule cells has progressed (white arrow). In addition, now there has been a substantial loss of CA3 pyramidal cells (black arrow). Much of the CA1 pyramidal cell population, however, remains intact (arrowhead). (D) By PD270 (9 months), neuronal loss within the hippocampal formation has progressed even further, and is now nearly total. Very few dentate granule cells remain alive (white arrow). Only a small patch of pyramidal cells can be identified (white arrowhead). The extensive pyramidal cell loss at this stage includes not only the CA3 subregion (black arrow), but also CA1 (black arrowhead). (E) Higher magnification from (B) demonstrates the beginnings of gliosis at age 2.5 months. The small darkly-stained cells with little cytoplasm (arrows) are astrocytes that are replacing lost neurons. (F) Higher magnification from (C) demonstrates that the density of glial cells (arrows) within the hippocampus has increased markedly by 5.5 months of age. (G) Higher magnification from (D) demonstrates that a dense glial scar (arrows) has replaced the neuronal populations of the hippocampal formation by 9 months of age. Magnification bars represent 400 μ m in A–D and 60 μ m in E–G.

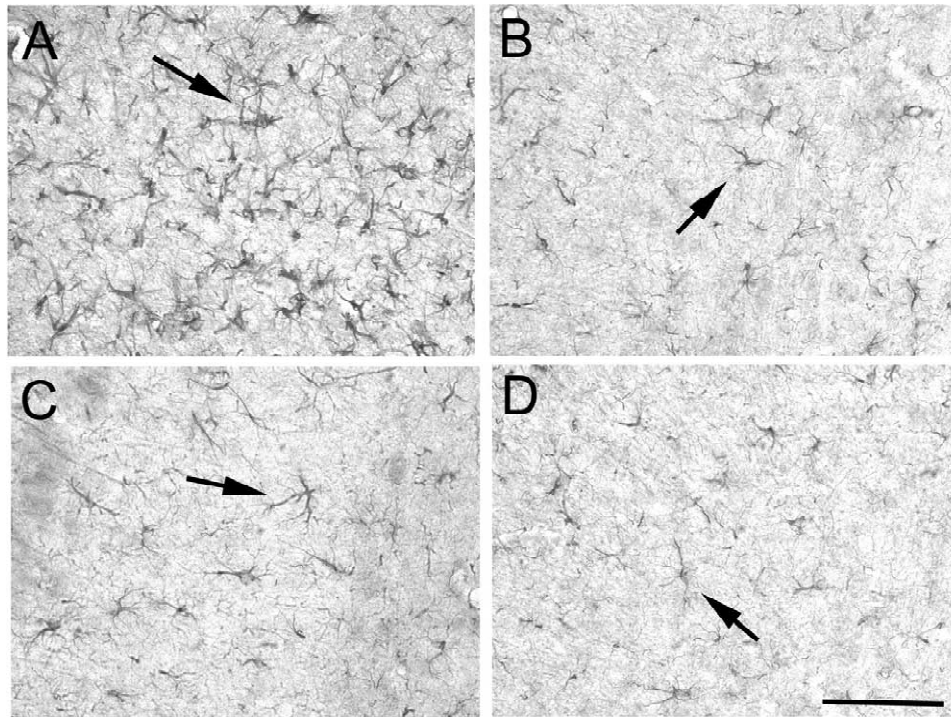


Fig. 7. Sections through the hippocampus and cerebral cortex stained immunohistochemically for glial fibrillary acidic protein (GFAP), a specific marker of astroglial cells. The sections were all derived from animals on PD165 and reveal an astrogliosis in the hippocampal formation of *Clcn3*^{-/-} mice. In each panel, the arrow points to an immunohistochemically labeled astrocyte. (A) Section through the dentate gyrus of a *Clcn3*^{-/-} mouse. The density of astrocytes in the dentate gyrus of the knockout mouse is much greater than in the *Clcn3*^{+/+} mouse (B). (B) Section through the dentate gyrus of wild type mouse. (C) Section through the cerebral neocortex of a *Clcn3*^{-/-} mouse. (D) Section through the cerebral neocortex of a wild type mouse. In the cerebral neocortex of the *Clcn3*^{-/-} mouse, the density of astrocytes is similar to that of the wild type mouse. No astrogliosis occurs in the neocortex of *Clcn3*^{-/-} or wild type mice. These observations demonstrate that an astrogliosis occurs in *Clcn3*^{-/-} mice, but only in the hippocampal formation, where the astroglial response accompanies neuronal loss. Magnification bar in D represents 40 μm in A, B, C, and D.

that depended on position along the septo–temporal axis. In contrast, brains of *Clcn3*^{+/-} mice appeared histologically normal at all time points examined. No degenerative processes or abnormalities of neural anatomy were evident in three *Clcn3*^{+/-} mice exceeding 600 days of age.

The structure of the hippocampal formation and of all other brain regions within the *Clcn3*^{-/-} mice appeared normal at PD23 (Fig. 6A), indicating that these animals generated a normal complement of central nervous system neurons, including those of the hippocampal formation, during prenatal and early postnatal life. However, by PD73 (Fig. 6B), a loss of neurons was evident in the hippocampal formation. At this time point, the neuronal dropout was most severe among the granule cells of the dentate gyrus. This loss of dentate granule cells substantially reduced the width of the dentate stratum granulosum. By PD165 (Fig. 6C), neuronal dropout from the hippocampal formation had worsened substantially and involved not only granule cells, but also pyramidal cells. At this time point, loss of pyramidal cells was more severe within the CA3 region than within CA1. In addition to neuronal loss, a second pathologic process, gliosis, was evident at this age. Within the regions in which neurons were lost, large numbers of small darkly-staining cells were apparent in Nissl-stained sections. The identity of these cells was confirmed as

astroglia in sections stained immunohistochemically for GFAP, an astrocyte-specific marker. Fig. 7 shows that the small cells contained GFAP, and the density of these labeled cells was substantially greater in the *Clcn3*^{-/-} hippocampus than in the control hippocampus. By PD270 (Fig. 6D), loss of neurons from the hippocampal formation was profound. A large proportion of neurons had been replaced by astrocytes (Fig. 6E–G). In contrast to the pattern at earlier time points, pyramidal cell loss was now extensive, not only in CA3, but also in the CA1 region.

Although pathologic changes ultimately occurred throughout the hippocampal formation, the time course of the pathology was a function of position along the septo–temporal axis. As shown in Fig. 8, neuronal cell loss occurred earlier in the septal (anterior) pole, than in the temporal (posterior) pole. By PD270 (9 months of age, Fig. 8), the entire anterior portion of the hippocampal formation had undergone neuronal degeneration, and all of the neurons had been replaced with astrocytes. In contrast, in the posterior hippocampus, a large proportion of pyramidal neurons remained identifiable. By 12 months of age, however, virtually all neurons of the hippocampal formation were lost. Degeneration of the hippocampal formation was accompanied by a progressive enlargement of the lateral ventricles (hydrocephalus ex vacuo). As

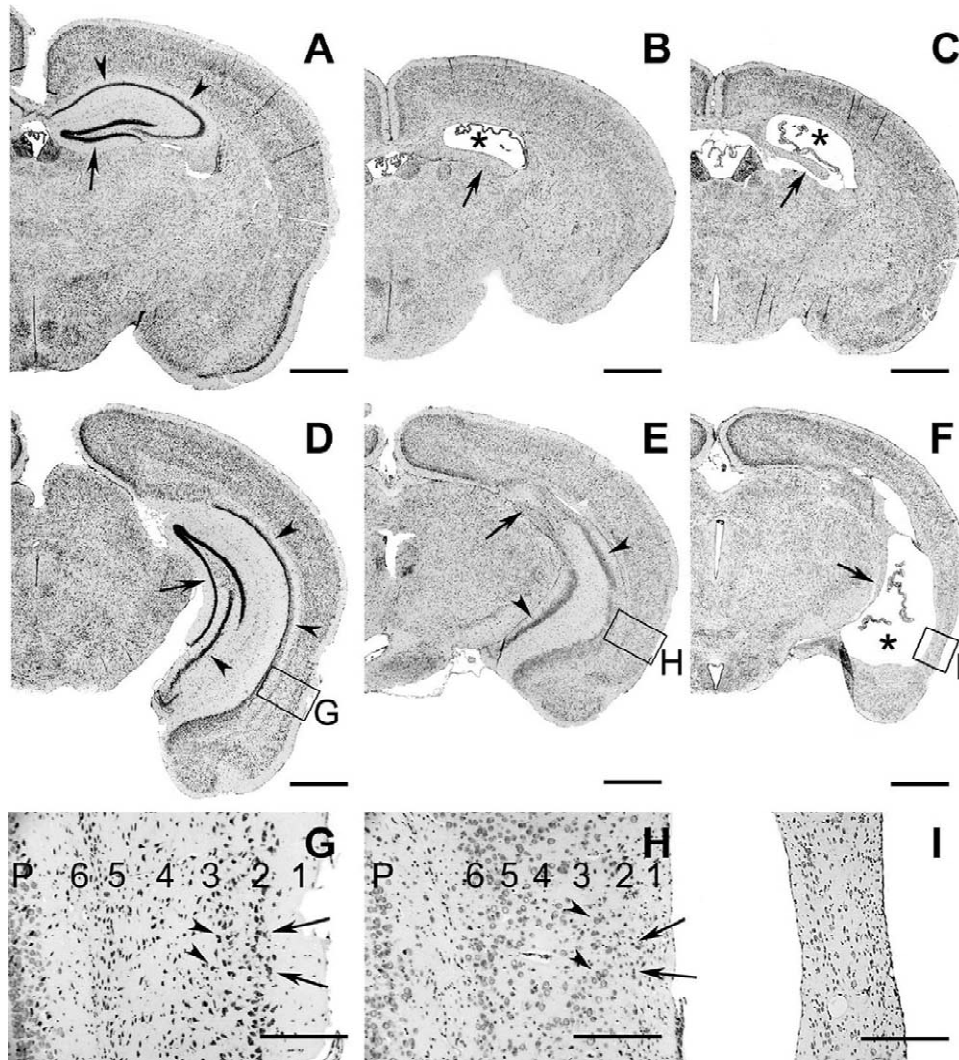


Fig. 8. Nissl-stained coronal sections through the cerebrum demonstrating that neuronal loss in the anterior hippocampal formation precedes neuronal loss in its posterior regions and that hippocampal cell loss is accompanied by ventriculomegaly and degeneration of the entorhinal cortex in *Clcn3*^{-/-} mice. Panels A, D, and G are from a 9-month-old wild type (*Clcn3*^{+/+}) mouse. Panels B, E, and H are from a 9-month-old knockout (*Clcn3*^{-/-}) mouse. Panels C, F and H are from a 12-month-old knockout mouse. (A) Section through the anterior forebrain of a 9-month-old *Clcn3*^{+/+} animal demonstrating the normal configuration of neurons within the dentate gyrus (arrow) and hippocampus (arrowheads). (B) Section through the anterior forebrain of a 9-month-old *Clcn3*^{-/-} mouse taken from the same anterior–posterior position as in (A) demonstrating that all neurons of the anterior hippocampal formation have degenerated and are now absent. The marked atrophy of the anterior hippocampal formation (arrow) is accompanied by lateral ventriculomegaly (asterisk). (C) Section through the anterior forebrain of a 12-month-old *Clcn3*^{-/-} mouse taken from the same anterior–posterior position as in (A) demonstrating advanced, but stable, pathology. The anterior hippocampal formation remains markedly atrophied (arrow), and the ventriculomegaly induced by the hippocampal degeneration remains evident (asterisk). (D) Section through the posterior forebrain of a 9-month-old *Clcn3*^{+/+} mouse demonstrating the normal configuration of the dentate gyrus (arrow) and hippocampal stratum pyramidale (arrowheads). The entorhinal cortex is located within the box. (E) Section through the posterior forebrain of the same 9-month-old *Clcn3*^{-/-} mouse whose anterior forebrain is shown in (B). This micrograph demonstrates that some neuronal loss has occurred within the posterior hippocampus, but not to the extent observed more anteriorly. The dentate gyrus has completely degenerated (arrow), but many pyramidal neurons of the hippocampus (arrowheads) remain viable at this age. The lateral ventricle is not enlarged in this plane of section, but is markedly enlarged more anteriorly (B). The entorhinal cortex (box) has a near-normal thickness at this age. (F) Section through the posterior forebrain of the same 12-month-old *Clcn3*^{-/-} mouse whose anterior forebrain is shown in (C). The entire posterior hippocampal formation, including the dentate gyrus and hippocampus proper, has degenerated and only a remnant of gliotic tissue (arrow) remains in its place. The entorhinal cortex (box) has selectively degenerated and is markedly reduced in thickness. The remainder of the cerebral cortex remains normal in thickness. The combined degeneration of the hippocampal formation and entorhinal cortex has led to a marked enlargement of the lateral ventricle (asterisk). (G) Inset from (D) demonstrating the normal six-layered configuration of the entorhinal cortex (1–6). Layer 2 stellate cells (arrows) are large hyperchromatic neurons that project to the dentate granule cells. Layer 3 pyramidal cells (arrowheads) constitute the thickest layer of the entorhinal cortex and project to hippocampal pyramidal cells. Stratum pyramidale (P) of the hippocampus lies deep to the entorhinal cortex. (H) Inset from (E) shows pathological changes within the entorhinal cortex of a 9-month-old *Clcn3*^{-/-} mouse. Layer 2 has selectively degenerated. The stellate cells that normally constitute layer 2 are absent and have been replaced by small cells (arrows) with the staining characteristics of astroglia. At this stage, the other cell layers remain essentially intact, including layer 3 pyramidal cells (arrowheads). (I) Inset from (F) shows dramatic neuronal loss and atrophy of the entorhinal cortex of a 12-month-old *Clcn3*^{-/-} mouse. Not only are the stellate cells of layer 2 absent, but so are the pyramidal cells of layer 3. The cytoarchitecture of the entorhinal cortex is markedly disrupted. Magnification bars represent 1 mm in A–F and 250 μ m in G–I.

shown in Fig. 8, because the degeneration of the hippocampal formation progressed from anterior to posterior, the ventriculomegaly progressed in this pattern as well.

In addition to the hippocampal formation, the entorhinal cortex also underwent degenerative changes (Fig. 8). Initially, the histology of the entorhinal cortex was normal. However, by 9 months of age, there was a specific loss of neurons from layer 2 of the entorhinal cortex. By 1 year of age, the loss of cells from the entorhinal cortex also included the neurons of layer 3. This degeneration of layers 2 and 3 resulted in a profound reduction in the thickness of the entorhinal cortex and in an exacerbation of the lateral ventriculomegaly. Outside of the hippocampus, the entorhinal cortex was the only portion of cerebral cortex that underwent evident pathologic change in *Clcn3*^{-/-} mice. As was true within the hippocampus, the entorhinal cortex also underwent a substantial gliosis as its neurons degenerated.

3.4. Behavioral responses to drugs affecting excitability or arousal

Midazolam, a benzodiazepine agonist at GABA_A receptors [21], was administered to young adult mice. One effect of midazolam is behavioral immobility, such that normal mice tend to sit prone in a ‘sphinx’-like position, maintaining an upright posture (i.e., not lying on their sides). To assess the strength of the benzodiazepine effect, the time-to-onset of immobility and the duration of immobility were measured. Initiation of either spontaneous walking or grooming while sitting upright defined the end of behavioral immobility. Mice lacking CIC-3 channels had a significantly reduced time-to-onset of midazolam-induced immobility (Fig. 9A) and a significantly increased duration of midazolam-induced immobility (Fig. 9B), compared to heterozygote and wild type mice. Complete loss of the righting reflex was the most striking feature of the response to midazolam by all of the *Clcn3*^{-/-} mice, and was never observed in *Clcn3*^{+/-} or *Clcn3*^{+/+} mice (Fig. 9C). This loss of righting reflex persisted for a

prolonged period of time in the *Clcn3*^{-/-} mice (52±4 min). Because loss of the righting reflex has been used as one measure of anesthetic effects in animals, we checked the reflex withdrawal of the lower limbs in response to brief toe-pinch, approximately every 10 min in all groups of mice. All three groups of mice retained the ability to respond briskly and promptly to toe pinch, a suprathreshold stimulus, throughout the study. There were no qualitative differences in the response of *Clcn3*^{-/-} mice to toe pinch, indicating no major impairment of reflex responses and no significant anesthetic-like effects. Although sedated, none of the mice appeared to be asleep during the study, as all mice kept their eyes open and periodically sniffed the air, moved a limb, or otherwise showed small indications of environmental awareness.

Four adult *Clcn3*^{-/-} mice were observed having spontaneous generalized tonic-clonic seizures during routine mouse colony care. One of these episodes resulted in the death of the mouse. Spontaneous seizures were never observed in *Clcn3*^{+/-} or *Clcn3*^{+/+} mice. Because of these qualitative observations, and more importantly, because hippocampal neuronal loss often is associated with epilepsy and with reduced seizure thresholds [6,23,37], we hypothesized that *Clcn3*^{-/-} mice would have lower thresholds for drug-induced seizures than *Clcn3*^{+/-} or *Clcn3*^{+/+} mice. We selected an age of 4–5 weeks, when *Clcn3*^{-/-} mice still have an essentially intact hippocampus and dentate gyrus, but at a time when neuronal irritability and excitability might be enhanced due to the early phase of neuronal degeneration. Pentylentetrazole (PTZ, 70 mg/kg, i.p.), an inhibitor of GABA_A receptors [51] was administered to conscious, drug-naïve mice (Fig. 10A). PTZ induced generalized seizures in 13/15 (86.7%) *Clcn3*^{+/-} mice (onset 215±56 s), in 7/8 (87.5%) of *Clcn3*^{+/+} mice (onset 280±112 s), but in only 1/8 (12.5%) of *Clcn3*^{-/-} mice (onset at 58 s). One mouse in each of the three groups died during a tonic generalized seizure. Thus, young *Clcn3*^{-/-} mice were significantly less susceptible to PTZ-induced generalized seizures compared to controls (Fig. 10A).

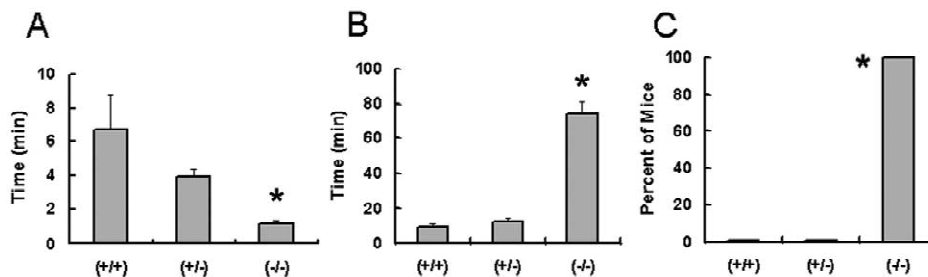


Fig. 9. *Clcn3*^{-/-} mice are highly sensitive to the effects of midazolam. Midazolam is a benzodiazepine that binds to and agonizes the GABA_A receptor. One behavioral effect of midazolam is immobility. The time-to-onset of immobility and the duration of immobility have been used to assess the strength of this effect. (*Clcn3*^{+/+}, n=6; *Clcn3*^{+/-}, n=12; *Clcn3*^{-/-}, n=6). (A) *Clcn3*^{-/-} mice have a substantially reduced time-to-onset of midazolam-induced immobility. (B) *Clcn3*^{-/-} mice have a markedly increased duration of midazolam-induced immobility compared to the other mice. (C) After a brief period of sitting immobile in a prone posture, all of the *Clcn3*^{-/-} mice exhibited loss of the righting reflex in response to midazolam, an effect which lasted 52±4 min. In contrast, none of the other mice exhibited this behavioral effect.

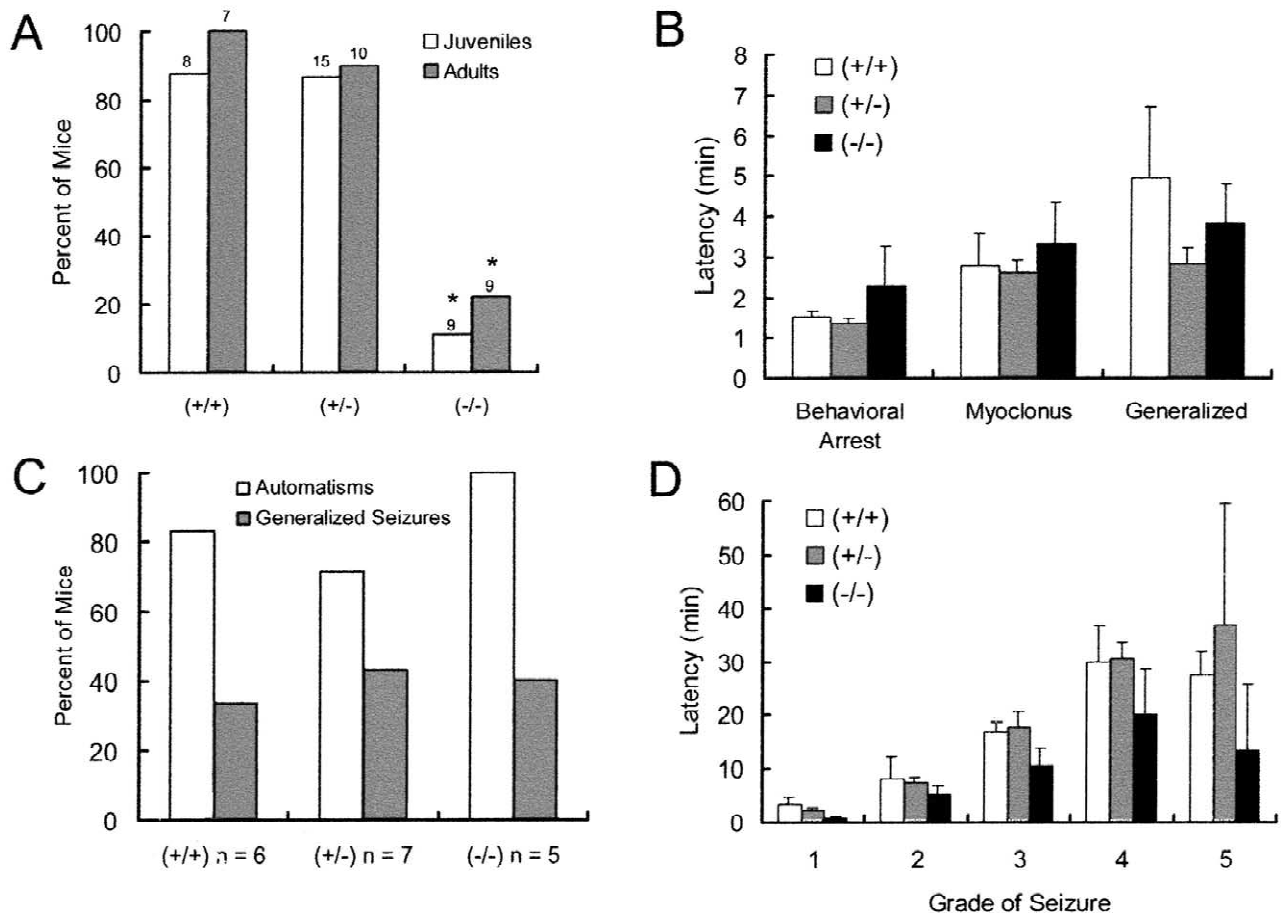


Fig. 10. Comparison of responses to two seizure-inducing drugs, PTZ and KA, which act by different mechanisms. (A) Percent of mice exhibiting generalized seizures in response to PTZ. Both juvenile and adult *Clcn3*^{-/-} mice are relatively resistant to PTZ-induced seizures compared to age-matched *Clcn3*^{+/-} and *Clcn3*^{+/+} mice within the two age ranges. (B) Latencies to first occurrence of behavioral arrest, myoclonic jerks, or generalized seizures in response to PTZ in the adult mice. Behavioral arrest and brief myoclonus occurred in nearly all mice in each of the three groups. (C) In response to KA, *Clcn3*^{-/-} mice exhibited complex behavioral automatisms (grades 3 and 4) or generalized seizures (grade 5) with similar incidences to *Clcn3*^{+/-} and *Clcn3*^{+/+} mice. (D) Latency to first occurrence of seizure-related phenomena in response to KA shows no significant differences between groups of mice. The grading system for KA responses was defined as follows. Grade 1: behavioral arrest, staring; grade 2: myoclonic jerks of limbs, head, neck, or thorax, or head nodding/swaying; grade 3: unilateral clonic activity, front or hindlimb pawing, may result in circling; grade 4: bilateral forelimb tonic or clonic activity (pawing the air, rearing, jumping, wobbling, falling); grade 5: generalized tonic/clonic activity with loss of postural tone, with or without death.

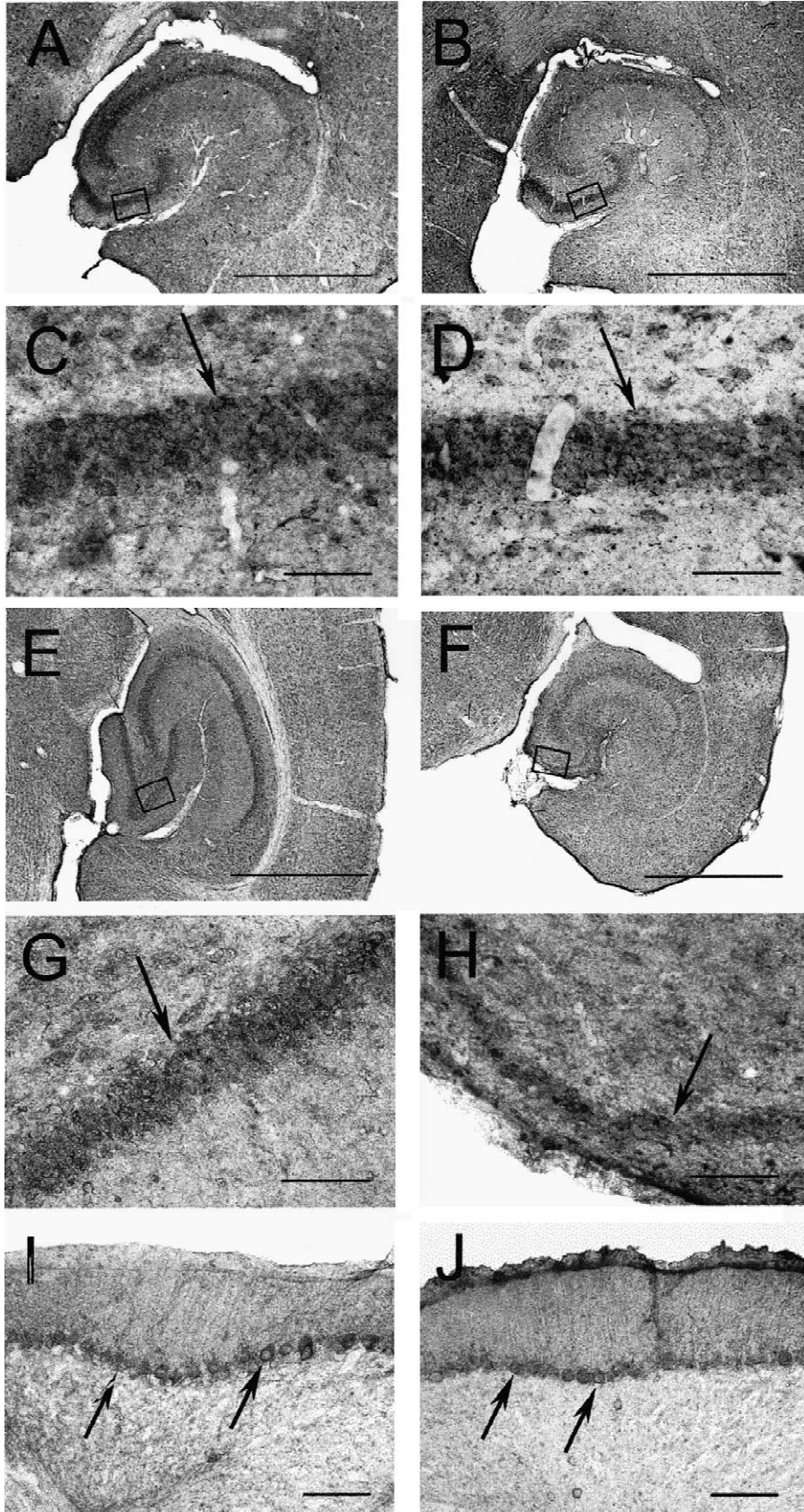
This relative resistance to PTZ persisted into adulthood, as indicated by subsequent tests on a separate group of mice aged 3–4 months (52.5 mg/kg, i.p.). Adult *Clcn3*^{-/-} mice were still significantly less susceptible to the effects of PTZ compared to *Clcn3*^{+/-} and *Clcn3*^{+/+} mice (Fig. 10A). The lower dose of PTZ was used in adult mice because the higher dose (70 mg/kg i.p.) was lethal across phenotypes: *Clcn3*^{-/-} mice ($n=2$) died in generalized seizures, as did *Clcn3*^{+/-} mice ($n=2$) and *Clcn3*^{+/+} mice ($n=2$). Increased sensitivity to PTZ in adults compared to juvenile animals has been shown in other rodent studies [6]. These data indicate that, although significantly less susceptible to the effects of PTZ at 52.5 mg/kg, adult *Clcn3*^{-/-} mice were capable of generating seizures in response to higher doses of PTZ.

KA (30 mg/kg, i.p.) was administered to 4–6-week-old mice to test whether the decreased susceptibility to seizures also applied to seizures induced by non-GABAergic

mechanisms. KA is an agonist of AMPA (non-NMDA) glutamate receptors [15] which are present on murine hippocampal pyramidal cells [71]. Mice lacking CIC-3 channels were as sensitive to KA-induced stereotypical automatisms and generalized seizures as were the heterozygous and wild type mice (Fig. 10B). No qualitative (grade of seizure activity) or quantitative (percent of mice exhibiting a grade of response, latency to onset of first occurrence) differences were seen in the response to KA among the three groups of mice.

3.5. GABA_A receptors and GAD-positive neurons in the hippocampal formation

Clcn3^{-/-} mice exhibited hippocampal degeneration and markedly abnormal responses to two agents whose site of action is the GABA_A receptor. Therefore, we investigated whether there might be changes in the density or dis-



tribution of GABA-synthesizing cells or of GABA_A receptors in the dentate gyrus and hippocampus.

Glutamic acid decarboxylase (GAD) is the enzyme that catalyzes production of GABA in neurons [40]. We assessed the presence of GAD-containing neurons by immunohistochemistry in brains from juvenile and young adult mice. On PD23, prior to the onset of evident neuronal degeneration, the pattern and intensity of GAD67 immunoreactivity was very similar in *Clcn3*^{-/-} mice (Fig. 11B, D) and wild type controls (Fig. 11A, C). This similarity suggested that GABAergic innervation of the dentate gyrus and hippocampus was initially normal. By early adulthood (PD73), when the dentate gyrus was actively degenerating, GAD67 immunoreactivity was markedly reduced in the dentate gyrus of *Clcn3*^{-/-} mice (Fig. 11F, H). Although the density of GAD67 staining remained normal, the total area of GAD67 staining within the dentate gyrus was substantially reduced, implying a loss of GABAergic neurons. In contrast, GAD67 immunoreactivity in the dentate gyrus of wild type mice remained prominent on PD73 (Fig. 11E, G). The alteration in GAD67 immunohistochemical staining in *Clcn3*^{-/-} mice was specific to the dentate gyrus. In the cerebellum, where no neuronal loss occurred, GAD67 staining of Purkinje cells at PD73 was identical in *Clcn3*^{-/-} (Fig. 11J) and *Clcn3*^{+/+} mice (Fig. 11I).

We next investigated whether there might be alterations in the density or distribution of GABA_A receptors in the hippocampus and dentate gyrus, possibly as a result of upregulation in response to diminished GABAergic input or to a hyperexcitable state. During the juvenile period (PD23), just prior to the onset of granule cell degeneration, the intensity of immunostaining for GABA_A receptors was increased on dentate granule cells of *Clcn3*^{-/-} mice (Fig. 12B, D) compared to controls (Fig. 12A, C), and also compared to the degree of staining in the CA1 and CA3 regions of the *Clcn3*^{-/-} brain. By early adulthood (PD73), while the dentate gyrus is actively degenerating, the intensity of immunostaining for GABA_A receptors was increased on the still-surviving cells of the dentate gyrus in of *Clcn3*^{-/-} mice (Fig. 12F, H), relative to controls (Fig. 12E, G). This alteration in the intensity of immunostaining for GABA_A receptors was confined to stratum granulosum, which is the initial site of neuronal dropout. Changes in the intensity of labeling for GABA_A receptors were never observed in hippocampal stratum pyramidale or in any other brain region.

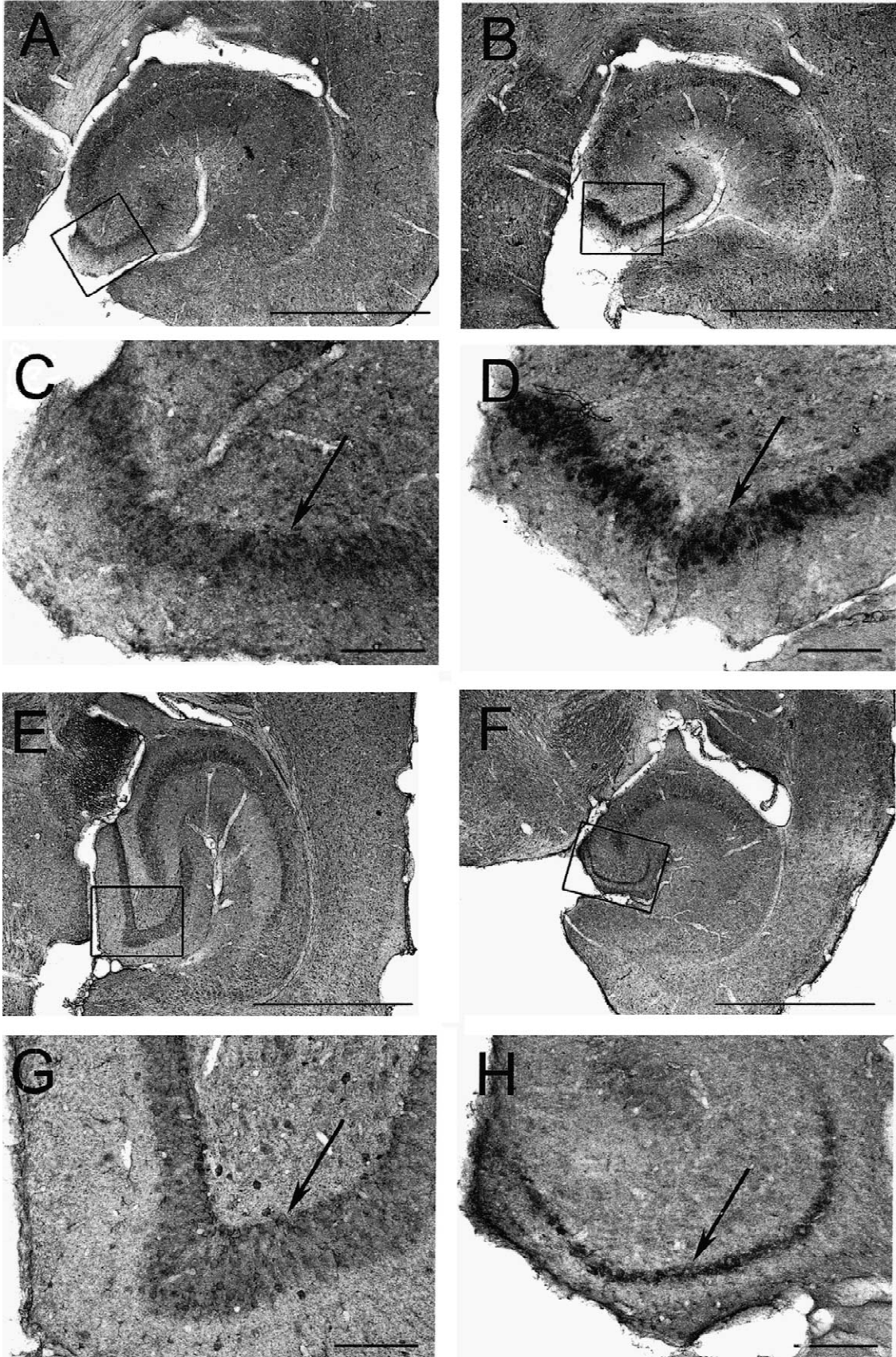
Quantitative assessment of the immunostaining confirmed the altered GABA_A receptor staining intensity within the dentate gyrus of *Clcn3*^{-/-} mice. As shown in Fig. 13, on both PD23 and PD73, the relative intensity of GABA_A receptor staining was significantly greater within the dentate gyrus of *Clcn3*^{-/-} mice than of *Clcn3*^{+/+} or *Clcn3*^{+/-} mice. This altered intensity of GABA_A receptor staining was confined to the dentate gyrus. Intensity of staining for GABA_A receptor did not differ significantly among genotypes within either the CA3 or CA1 hippocampal subfields at either age.

In contrast to the substantial differences in GABA_A receptor staining, GAD-67 immunostaining intensity did not differ significantly among the genotypes (Fig. 13C, D). The relative density of GAD-67 staining did not differ significantly in any of the analyzed regions of the hippocampus at either age.

4. Discussion

In order to provide insight into the function of CIC-3 chloride channels, we created a line of mice lacking this protein. *Clcn3*^{-/-} mice display a variety of phenotypic features, including poor growth, sudden death without obvious prodrome, waddling gait, absence of normal escape extension behavior, kyphosis, blindness, and altered neurologic responses to drugs that affect GABA_A neurotransmission. Seizures were observed in four *Clcn3*^{-/-} mice and the lethality of one of these events suggests that at least a portion of the early mortality in these animals is due to seizures. No abnormalities in serum electrolytes or acid–base status were identified that might predispose to neuronal hyperexcitability. Although baseline serum glucose was lower in *Clcn3*^{-/-} mice than in wild type mice, this mild reduction in serum glucose seems unlikely to result in seizures. Many of the phenotypic characteristics of the *Clcn3*^{-/-} mice are clearly related to gross neurodegenerative changes in the retina and hippocampus, while others may be the result of more subtle functional impairments in other brain regions. The CNS pathology that we observe is similar to that seen in two other independently-produced lines of *Clcn3*^{-/-} mice [58,72]. There is rapid postnatal degeneration of retinal photoreceptors and progressive degeneration of hippocampal neurons. However, the progression of hippocampal degeneration in our *Clcn3*^{-/-} mice differs both temporally (much slower:

Fig. 11. In *Clcn3*^{-/-} mice, degeneration of the dentate gyrus is accompanied by a reduction in glutamic acid decarboxylase (GAD) immunoreactivity in the dentate gyrus. (A)–(D) In juvenile mice (PD23, before the onset of neuronal degeneration), the pattern and intensity of GAD67 immunoreactivity is very similar in *Clcn3* knockout mice (B and D) as in wild type (A and C), suggesting that GABA-ergic innervation of the dentate gyrus is initially normal. (E)–(H) By early adulthood (PD73, when the dentate gyrus is actively degenerating), GAD immunoreactivity in the dentate gyrus is markedly reduced in the knockout mice (F and H) as the dentate gyrus contracts in size (though the intensity of the staining remains normal). GAD immunoreactivity in the dentate gyrus of control mice remains prominent (E and G). (I)–(J) GAD immunoreactivity in the cerebellar Purkinje cells of adult *Clcn3*^{-/-} mice (J) is similar to that of wild type mice (panel I). Arrows point to stratum granulosum in C, D, G and H and to Purkinje cells in I and J. Magnification bars represent 1 mm in A, B, E, and F; 50 μm in C, D, G and H; and 100 μm in I and J.



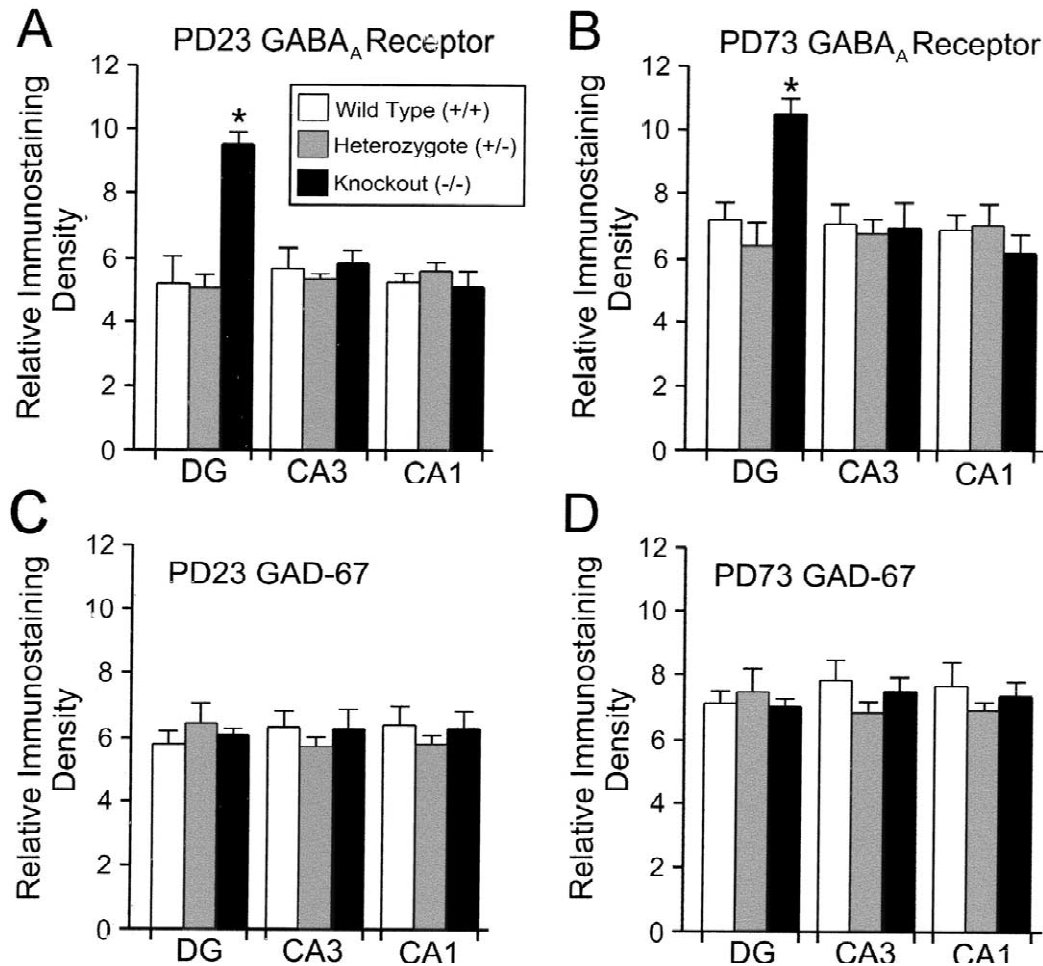


Fig. 13. Relative densities of immunohistochemical staining for GABA_A receptor and GAD-67 within subregions of the hippocampal formation in juvenile and young adult mice. (A) Relative intensity of staining for GABA_A receptor on PD23. Within the dentate gyrus, the relative intensity of staining is significantly greater in knockout mice than in wild type or heterozygous mice. In contrast, within CA3 and CA1, staining intensity for GABA_A receptor is not significantly different among the genotypes. * Significantly different from wild type and heterozygous mice ($P < 0.05$). (B) Relative intensity of staining for GABA_A receptor on PD73. As was true during the juvenile period, the relative density of GABA_A receptor staining is significantly increased within the dentate gyrus in $Clcn3^{-/-}$ mice, compared to wild type and heterozygous mice. Intensity of staining within CA3 and CA1 did not differ significantly among the genotypes. * Significantly different from wild type and heterozygous mice ($P < 0.05$). (C) Relative intensity of staining for GAD-67 on PD23. The density of staining did not differ among the genotypes in any of the hippocampal subregions analyzed. (D) Relative intensity of staining for GAD-67 on PD73. As was true during the juvenile period, the density of staining for GAD-67 did not differ among the genotypes in any of the brain regions.

months vs. weeks) and spatially (dentate gyrus to CA1 rather than CA1 to dentate) from that reported previously [58]. In addition, we report that the hippocampal neuronal loss is accompanied by a progressive astrogliosis and by a profound secondary loss of neurons from the entorhinal cortex.

4.1. Implications for exocytosis and granule acidification

$Clcn3^{-/-}$ mice display several phenotypic characteris-

tics that may or may not be related to degenerative changes in the CNS. For example, growth retardation is remarkable, and older adult $Clcn3^{-/-}$ animals clearly have diminished body fat. This leanness may account for the lower baseline blood glucose levels and more rapid recovery from a glucose load than was observed in the control animals. Measurement of insulin levels in a separate group of fasting mice did not yield significant differences between $Clcn3^{-/-}$ and $Clcn3^{+/+}$ mice. The ability of $Clcn3^{-/-}$ animals to handle glucose is relevant

Fig. 12. Intensity of GABA_A receptor immunostaining is increased in the dentate gyrus of juvenile and adult $Clcn3^{-/-}$ mice. (A)–(D) During the late juvenile period (PD23, just prior to the onset of granule cell degeneration), the intensity of immunostaining for GABA_A receptors is increased on dentate granule cells of $Clcn3^{-/-}$ mice (B and D) relative to wild type mice (A and C). (E)–(H) By early adulthood (PD73, while the dentate gyrus is actively degenerating), the intensity of immunostaining for GABA_A receptors is increased on the still-surviving cells of the dentate gyrus in $Clcn3^{-/-}$ mice (F and H), relative to wild type mice (E and G). Arrows point to stratum granulosum in C, D, G and H. Magnification bars represent 1 mm in A, B, E, and F; and 100 μ m in C, D, G, and H.

in view of the report that CIC-3 is involved in the acidification of insulin granules in preparation for exocytosis [3]. Acidification is a decisive step in ATP-dependent priming of insulin granules for exocytosis. Agents that prevent transgranular chloride fluxes, such as the chloride channel blocker DIDS and an antibody against CIC-3 channels, inhibit acidification and priming. Based on those findings, loss of the CIC-3 protein might have been predicted to inhibit the priming process *in vivo*, reduce serum insulin levels, and cause hyperglycemia, but this was not the case in *Clcn3*^{-/-} mice.

Although *Clcn3*^{-/-} mice do not exhibit the hyperglycemia predicted by the role of CIC-3 in insulin granules [3], other factors may affect the overall regulation of serum glucose in these animals. In interpreting all of the phenotypic features observed in these mice, it is important to consider the possibility that expression of other chloride channels or chloride transport proteins might be altered to compensate for the loss of CIC-3. Candidates for such compensatory changes are CIC-4 or CIC-5, proteins related structurally to CIC-3. Previous work did not reveal upregulation of CIC-4 or CIC-5 expression in brains of *Clcn3*^{-/-} mice [58].

4.2. Abnormalities of gait and the escape extension reflex

The *Clcn3*^{-/-} mouse's constellation of kyphosis, waddling gait, and rear-leg folding behavior upon suspension by the tail, resembles the triad of features displayed by a mouse model of Duchenne muscular dystrophy [13]. We initially hypothesized that these features of *Clcn3*^{-/-} mice were secondary to muscular weakness. However, we detected no weakness in forelimb grip strength in *Clcn3*^{-/-} mice (data not shown) and observed no light-microscopic evidence of skeletal muscle myopathy in *Clcn3*^{-/-} mice. Creatine kinase levels were not elevated in either young adult or older adult *Clcn3*^{-/-} mice. These findings do not support a primary abnormality of muscle function.

In the absence of a myopathy, the gait abnormality and absence of hindlimb escape extension may be related to impaired vestibular or cerebellar function in *Clcn3*^{-/-} mice [30,60]. The complete loss of the righting reflex induced by midazolam in *Clcn3*^{-/-} mice further suggests altered cerebellar function. This possibility is consistent with the abnormal rota-rod performance previously described in *Clcn3*^{-/-} mice [58,72]. In our studies, light microscopy did not reveal any abnormality of cerebellar histology although *Clcn3* is highly expressed in this brain region [27].

4.3. Neuronal degeneration begins in the dentate gyrus and proceeds to CA3, CA1, and the entorhinal cortex

Degeneration of the retina and hippocampal formation in *Clcn3*^{-/-} mice have been reported previously [58,72]. We

confirm a rapid retinal degeneration with virtually complete loss of the outer retinal segments by 23 days of age. However, in contrast to previous findings, we observe a much slower time course of hippocampal degeneration that occurs over months, instead of weeks, and that progresses in a different sequence among neuronal subpopulations. Our new findings show that absence of the CIC-3 voltage-gated chloride channel induces: (1) degeneration and gliosis of the dentate gyrus and hippocampus that progresses from anterior to posterior, (2) sequential loss of neuronal subpopulations that begins in the dentate gyrus, and progresses to involve CA3, followed by CA1, (3) a delayed-onset degeneration of layers 2 and 3 of the entorhinal cortex, (4) greatly decreased sensitivity to PTZ-induced seizures in both juvenile and adult mice, (5) no change in vulnerability to KA-induced seizures, (6) prolonged action of, and increased sensitivity to, midazolam, and (7) a decrease in the number of GABA-synthesizing (GAD67-positive) cells within the dentate gyrus which is temporally preceded by (8) increased GABA_A receptor immunoreactive staining in the dentate gyrus.

Like the hippocampal formation and retina, the entorhinal cortex also degenerates in *Clcn3*^{-/-} mice. However, unlike the hippocampal formation and retina, where the neurodegeneration is likely due directly to a defect in the *Clcn3* gene, the entorhinal cortex degeneration is probably a secondary pathologic change, due to the loss of synaptic target cells within the hippocampal formation. Large stellate neurons constitute layer 2 of the entorhinal cortex and normally project to the granule cells of the dentate gyrus [57]. These layer 2 neurons are the first cells of the entorhinal cortex to degenerate in *Clcn3*^{-/-} mice, and the onset of this degeneration follows the loss of dentate granule cells. Pyramidal cells constitute layer 3 of the entorhinal cortex and normally project to hippocampal pyramidal cells [56]. These layer 3 neurons initially remain viable in *Clcn3*^{-/-} mice following the loss of entorhinal stellate cells and of dentate granule cells, but they degenerate following the loss of hippocampal pyramidal cells. Thus, both the time course and the pattern of cell loss within the entorhinal cortex suggest that neuronal death in that structure represents retrograde trans-synaptic degeneration as a result of target removal.

The entorhinal neuronal loss may be of substantial importance to the behavior and biology of *Clcn3*^{-/-} mice. Pathologic changes relatively confined to the entorhinal cortex have been observed in schizophrenia [2] and in Alzheimer's disease [25] and are believed to underlie many of the behavioral deficits marking these diseases. Neuronal loss from layer 3 of the entorhinal cortex occurs in humans with temporal lobe epilepsy and hippocampal sclerosis [17] and in multiple animal models of these diseases [16,69]. In animal models of temporal lobe epilepsy, the onset of spontaneously recurring seizures has been tied to neuronal loss from layer 3 of the entorhinal cortex [69]. In the *Clcn3*^{-/-} mice, the pathology of the

entorhinal cortex may contribute to the seizure disorder, and ultimately, to the death of some of these animals.

Hippocampal neuronal cell loss is accompanied by substantial astrogliosis. The astrogliosis is relevant to the utility of the *Clcn3*^{-/-} mouse as a model for human hippocampal sclerosis. Hippocampal sclerosis is a major cause of temporal lobe epilepsy in humans and is defined not only by the loss of hippocampal neurons, but also by the replacement of hippocampal neurons by astrocytes [63]. The cause of hippocampal sclerosis is unknown, but genetic factors may play a role [5].

Our findings that hippocampal degeneration begins in the dentate gyrus and that the altered GABA_A receptor and GAD67 immunostaining are both localized to the dentate gyrus all suggest that events or conditions specifically within the dentate gyrus may be of particular importance to the behavioral and histologic abnormalities observed in *Clcn3*^{-/-} mice. Again, these data may be relevant to human hippocampal sclerosis, in which pathologic changes in the dentate gyrus are both prominent and contributory to the disease process [9,22,45].

4.4. Altered responses to PTZ and midazolam suggest GABA_A receptor upregulation

The observation of spontaneous seizures in mice with hippocampal degeneration suggested that these two phenomena might be related. The hippocampal formation is one of the most epileptogenic regions of the rodent brain [37,59] and lesions at any site within it can lower the threshold for seizures and induce epilepsy [6,37]. Furthermore, the hippocampal formation is involved in the major motor seizures induced by PTZ [59]. We hypothesized that *Clcn3*^{-/-} mice would have a lowered threshold to PTZ-induced seizures. Surprisingly, both young (4–5 weeks) and older (3–4 months) mice exhibited a marked resistance to PTZ-induced seizures compared to age-matched controls. This could be due to interruption of the circuitry of the hippocampal formation at very early stages of degeneration (i.e., synaptic disruption) that is not yet evident under light microscopy. This might render the network properties of the neural circuits insufficient to support the ensemble excitation and re-excitation necessary for generation of limbic seizures. However, the absence of qualitative or quantitative differences between *Clcn3* genotypes in the response to KA shows that this circuitry is sufficiently intact to generate and sustain seizures. These findings indicate that *Clcn3*^{-/-} mice are capable of generating seizures and have functional AMPA/KA glutamate receptors. Therefore, the reduced susceptibility to PTZ-induced seizures probably is not caused by an insufficiency in either connectional circuitry or in glutamatergic excitation, but may be due to a change in GABAergic neurotransmission.

Clcn3^{-/-} mice are extremely sensitive to, and exhibit a markedly prolonged recovery from, midazolam, a benzodiazepine that enhances activity of GABA_A receptors. An

increased sensitivity to midazolam, combined with resistance to PTZ, an inhibitor of GABA_A receptors, strongly point to an abnormality in GABA neurotransmission. Upregulation of GABA neurotransmission has been shown to suppress hippocampal excitability in another experimental model, a line of transgenic mice overexpressing superoxide dismutase [32]. However, those transgenic mice were highly resistant to induction of KA seizures, in contrast to normal KA sensitivity in *Clcn3*^{-/-} mice.

Aberrant GABAergic function may occur in other CNS regions beyond the hippocampal formation, and may account for some of the phenotypic abnormalities in *Clcn3*^{-/-} mice. In particular, GABA-mediated excitation is present within spinal pathways and exerts an influence on spinal motor neurons. The kyphosis observed in *Clcn3*^{-/-} mice may be due to abnormal spinal influences on the paraspinal musculature.

Loss of a synaptic vesicular chloride conductance may have complex effects on GABA uptake because GABA uptake is dependent upon both the proton gradient and the electrical gradient across the vesicular membrane [44]. Absence of a vesicular chloride conductance is expected to decrease the proton gradient but increase the electrical gradient. Miniature inhibitory postsynaptic currents (GABAergic) were not altered in CA1 pyramidal cells from *Clcn3*^{-/-} mouse pups; however, this was not tested in granule cells from the dentate gyrus [58]. It remains to be determined how the loss of ClC-3 channels affects GABAergic neurotransmission in a complex neural network.

The immunohistochemical data showed a decrease in the number of GABA-synthesizing (GAD67-positive) cells, which is temporally preceded by increased GABA_A receptor immunoreactive staining in the dentate gyrus. In combination with the PTZ and midazolam data, these neurohistological findings support the hypothesis of impaired GABAergic neurotransmission and secondary upregulation of post-synaptic GABA_A receptors.

4.5. Sequence of hippocampal degeneration reflects its circuitry

The progression of regional neuronal dropout (dentate gyrus to CA3 to CA1) follows the pathway of excitatory circuitry of the hippocampal formation. The dentate gyrus is the major recipient of extra-hippocampal afferent input that comes from the entorhinal cortex via the perforant pathway. Dentate gyrus granule cells project mossy fibers to CA3 pyramidal cells, which in turn project to CA1 pyramidal cells via Schaffer collaterals [4]. This unidirectional dentate gyrus to CA3 to CA1 projection is termed the 'trisynaptic circuit' [68]. The matching of ordered neuronal dropout to this connectional anatomy suggests that anterograde transynaptic degeneration may underlie some of the neuronal loss in *Clcn3*^{-/-} mice [10,70]. The subiculum is a major recipient of hippocampal outflow and projects strongly back to the entorhinal

cortex. This completes an excitatory re-entrant loop, which provides recurrent enhancement of synaptic connections at all sites of the circuit, and could facilitate excitotoxicity. Although the intrinsic circuitry of the hippocampal formation is quite uniform throughout its septo–temporal extent, important differences in its afferent and efferent connections exist along its longitudinal axis [67,68]. The major inputs to posterior hippocampus are derived from the medial entorhinal cortex, amygdala and interpeduncular nuclei. In contrast, chief sources of afferent input to the anterior hippocampus arise from lateral entorhinal cortex, perirhinal cortex and raphe nuclei. Differences in time course of neurodegeneration between the anterior and posterior portions of the hippocampus may be related to these differences in circuitry.

Under normal conditions, excitotoxicity is prevented by inhibitory interneurons, whose principal transmitter is GABA. Loss or dysfunction of these inhibitory interneurons due to the absence of the CIC-3 chloride channel could render the granule cells and pyramidal cells vulnerable to excitotoxic cell death. A defect in GABA_A-mediated signaling, perhaps combined with an increase in glutamatergic (excitatory) signaling [58] in hippocampal pyramidal cells may provide a dual mechanism for excitotoxic neurodegeneration.

The cause of the disparities between lines of *Clcn3*^{-/-} mice in the rate and anatomic sequence of neuronal loss is not obvious. Our line of *Clcn3*^{-/-} mice was nominally created on the same C57BL/6×129SV genetic background as the *Clcn3*^{-/-} mouse of Stobrawa et al. [58]. Genetic drift between C57BL/6 mice obtained from different suppliers could result in different alleles of modifier genes for the *Clcn3*^{-/-} phenotype. Breeding of both colonies into a ‘pure’ C57BL/6 background may resolve these divergent phenotypes. In addition, subtle differences in diet or environment could contribute to the variation in phenotype between colonies. It has recently been proposed that the loss of CIC-3 produces a generalized abnormality in the protein degradation pathway [72]. In some respects, the *Clcn3*^{-/-} phenotype as described by Yoshikawa et al. bears similarities to human neuronal ceroid lipofuscinosis (NCL or Batten Disease), which is associated with progressive diffuse neurodegeneration, seizures and blindness [64]. Although focal hippocampal injury is not a characteristic of the human disease, it has been proposed that neuronal death in NCL is related to excitotoxicity caused by GABAergic cell loss [64].

If CIC-3 does normally function in neuronal membranes, loss of a surface chloride conductance could facilitate excitotoxicity by depolarizing resting membrane potential or impairing repolarization. An additional consideration is the fact that GABA_A receptor activation can be excitatory in the neonatal period [11] or when stimulation is prolonged [54]. An increase in KCC2 expression alters chloride equilibrium potential within the first 2 weeks of life. This upregulation of KCC2 renders GABA_A currents inhibitory [20,46]. If this transition were delayed or

prevented, it could lead to a primary excitation abnormality associated with enhanced GABAergic stimulation. Similarly, if increased GABA_A receptor expression is a primary problem related to the loss of CIC-3, this increased receptor density might convert normal levels of GABA stimulation from inhibitory to excitatory and contribute directly to excitotoxicity. The possibility that direct GABA-mediated excitation causes excitotoxicity seems less likely in view of our observation that GABA_A receptor activation by midazolam continues to produce sedation in the adult *Clcn3*^{-/-} mouse, and this effect is even enhanced, compared to controls.

4.6. Significance and conclusions

In summary, mice lacking CIC-3 exhibit a complex phenotype associated with progressive degeneration of the hippocampal formation and retina. Selective loss of neurons from the hippocampal formation and entorhinal cortex, accompanied by progressive gliosis, mimics the pathologic findings in human temporal lobe epilepsy. These similarities suggest that the *Clcn3*^{-/-} mouse may be a valuable model system for the study of hippocampal sclerosis. We tested the hypothesis that hippocampal degeneration is associated with a lower seizure threshold to PTZ and kainate but found no convincing evidence to support this proposal. *Clcn3*^{-/-} mice have no metabolic abnormalities that would predispose to seizures and these mice are resistant to PTZ-induced convulsions. They do not differ from control animals in their susceptibility to KA-induced seizures. Resistance to PTZ effects, increased sensitivity to benzodiazepines, and enhanced immunohistochemical staining that precedes major neuronal loss, when taken together, suggest that GABA_A receptors are upregulated. GABA_A receptor upregulation in the hippocampal formation remains to be confirmed by electrophysiological and/or biochemical means.

We recently reported that vascular function is impaired in the *Clcn3*^{-/-} mouse [14]. This finding raises the possibility that neuronal degeneration could be at least partially related to aberrations of vascular control of blood flow which could trigger—or exacerbate—processes of excitotoxicity in the hippocampal formation. It is well-known that the hippocampus is among the most sensitive regions of the brain to anoxic or ischemic injury [39]. Also, it is intriguing that intracellular chloride concentration increases in hippocampal pyramidal neurons subjected to acute oxidative stress [47]. Loss of a membrane chloride conductance could interact adversely with such processes. These speculations regarding the role of CIC-3-mediated vascular effects on the brain are under investigation.

Acknowledgements

We thank Jolonda Mahoney, Ruth Swiderski, Ronald D. Cohn and Andrew Lotery for technical assistance. We also

wish to thank Margaret Malik, Cheryl Zimmerman and Sarah Lilly, for assistance with breeding, genotyping, and maintenance of the mouse colony. Grant Support NIH HL62483 (F.S.L.), Children's Health Research Center at the University of Iowa NIH P30-HD 27748 (Frank Morriss, B.C.S., D.J.B.), NIH HL07121-Cardiovascular Interdisciplinary Research Fellowship Program (L.W.D.), NIH NS02007 (D.J.B.), the John Martin Fund for Neuroanatomical Research (D.J.B.), the Children's Miracle Network (D.J.B., B.C.S.), and the March of Dimes Birth Defects Foundation (1-FY01-217, D.J.B.).

References

- [1] D.A. Adler, E.I. Rugarli, P.A. Lingenfelter, K. Tsuchiya, D. Poslinski, H.D. Liggitt, V.M. Chapman, R.W. Elliott, A. Ballabio, C.M. Distche, Evidence of evolutionary up-regulation of the single active X chromosome in mammals based on Clc4 expression levels in *Mus spretus* and *Mus musculus*, *Proc. Natl. Acad. Sci. USA* 94 (1997) 9244–9248.
- [2] S.E. Arnold, B.T. Hyman, G.W. Van Hoesen, A.R. Damasio, Some cytoarchitectural abnormalities of the entorhinal cortex in schizophrenia, *Arch. Gen. Psychiatry* 48 (1991) 625–632.
- [3] S. Barg, P. Huang, L. Eliasson, D.J. Nelson, S. Obermuller, P. Rorsman, F. Thevenod, E. Renstrom, Priming of insulin granules for exocytosis by granular Cl⁻ uptake and acidification, *J. Cell Sci.* 114 (2001) 2145–2154.
- [4] S.A. Bayer, Hippocampal region, in: G. Paxinos (Ed.), *The Rat Nervous System, Forbrain and Midbrain*, Vol. 1, Academic Press, New York, 1985, pp. 335–352.
- [5] S.F. Berkovic, G.D. Jackson, The hippocampal sclerosis whodunit: enter the genes, *Ann. Neurol.* 47 (2000) 557–558.
- [6] D.J. Bonthius, J. Woodhouse, N.E. Bonthius, D.A. Taggard, E.W. Lothman, Reduced seizure threshold and hippocampal cell loss in rats exposed to alcohol during the brain growth spurt, *Alcohol Clin. Exp. Res.* 25 (2001) 70–82.
- [7] G. Borsani, E.I. Rugarli, M. Tagliatela, C. Wong, A. Ballabio, Characterization of a human and murine gene (CLCN3) sharing similarities to voltage-gated chloride channels and to a yeast integral membrane protein, *Genomics* 27 (1995) 131–141.
- [8] M.R. Bosl, V. Stein, C. Hubner, A.A. Zdebik, S.E. Jordt, A.K. Mukhopadhyay, M.S. Davidoff, A.F. Holstein, T.J. Jentsch, Male germ cells and photoreceptors, both dependent on close, degenerate upon ClC-2 Cl⁻ channel disruption, *EMBO J.* 20 (2001) 1289–1299.
- [9] R.S. Briellmann, R.M. Kalnins, S.F. Berkovic, G.D. Jackson, Hippocampal pathology in refractory temporal lobe epilepsy: T2-weighted signal change reflects dentate gliosis, *Neurology* 58 (2002) 265–271.
- [10] C.W. Chang, Evident trans-synaptic degeneration of motor neurons after stroke: a study of neuromuscular jitter by axonal microstimulation, *Electroencephalogr. Clin. Neurophysiol.* 109 (1998) 199–202.
- [11] E. Cherubini, J.L. Gaiarsa, Y. Ben-Ari, GABA: an excitatory transmitter in early postnatal life, *Trends Neurosci.* 14 (1991) 515–519.
- [12] G.H. Clayton, K.J. Staley, C.L. Wilcox, G.C. Owens, R.L. Smith, Developmental expression of ClC-2 in the rat nervous system., *Dev. Brain Res./IBR*, in press.
- [13] A.E. Deconinck, J.A. Rafael, J.A. Skinner, S.C. Brown, A.C. Potter, L. Metzinger, D.J. Watt, J.G. Dickson, J.M. Tinsley, K.E. Davies, Utrophin-dystrophin-deficient mice as a model for Duchenne muscular dystrophy, *Cell* 90 (1997) 717–727.
- [14] L.W. Dickerson, T.J. Barna, B.C. Schutte, X.R. Cao, B. Yang, F.S. Lamb, Decreased reactivity to norepinephrine (NE) in aortae from male ClC3 (-/-) mice, *FASEB J.* 15 (2001) A114.
- [15] R. Dingledine, C.J. McBain, Glutamate and aspartate, in: B.W.A.G.J. Siegel, R.W. Albers, S.K. Fisher, M.D. Uhler (Eds.), *Basic Neurochemistry: Molecular, Cellular and Medical Aspects*, 6th Edition, Lippincott-Raven, Philadelphia, PA, 1999, pp. 315–333, Chapter 15.
- [16] F. Du, T. Eid, E.W. Lothman, C. Kohler, R. Schwarcz, Preferential neuronal loss in layer III of the medial entorhinal cortex in rat models of temporal lobe epilepsy, *J. Neurosci.* 15 (1995) 6301–6313.
- [17] F. Du, W.O. Whetsell Jr., B. Abou-Khalil, B. Blumenkopf, E.W. Lothman, R. Schwarcz, Preferential neuronal loss in layer III of the entorhinal cortex in patients with temporal lobe epilepsy, *Epilepsy Res.* 16 (1993) 223–233.
- [18] D. Duan, S. Cowley, B. Horowitz, J.R. Hume, A serine residue in ClC-3 links phosphorylation–dephosphorylation to chloride channel regulation by cell volume, *J. Gen. Physiol.* 113 (1999) 57–70.
- [19] D. Duan, C. Winter, S. Cowley, J.R. Hume, B. Horowitz, Molecular identification of a volume-regulated chloride channel, *Nature* 390 (1997) 417–421.
- [20] K. Ganguly, A.F. Schinder, S.T. Wong, M. Poo, GABA itself promotes the developmental switch of neuronal GABAergic responses from excitation to inhibition, *Cell* 105 (2001) 521–532.
- [21] W.R. Hobbs, T.W. Rall, T. Verdoorn, Hypnotics and sedatives; ethanol, in: L.E.L.J.G. L.E.L.J.G. Hardman, P.B. Molinoff, R.W. Ruddan, A. Goodman Gilman (Eds.), *Goodman & Gilman's The Pharmacological Basis of Therapeutics*, 9th Edition, McGraw-Hill, New York, 1996, pp. 361–396, Chapter 17.
- [22] C.R. Houser, Granule cell dispersion in the dentate gyrus of humans with temporal lobe epilepsy, *Brain Res.* 535 (1990) 195–204.
- [23] R.Q. Hu, S. Koh, T. Torgerson, A.J. Cole, Neuronal stress and injury in C57/BL mice after systemic kainic acid administration, *Brain Res.* 810 (1998) 229–240.
- [24] P. Huang, J. Liu, A. Di, N.C. Robinson, M.W. Musch, M.A. Kaezel, D.J. Nelson, Regulation of human ClC-3 channels by multifunctional Ca²⁺/calmodulin dependent protein kinase, *J. Biol. Chem.* 276 (2001) 20092–20100.
- [25] B.T. Hyman, G.W. Van Hoesen, L.J. Kromer, A.R. Damasio, Perforant pathway changes and the memory impairment of Alzheimer's disease, *Ann. Neurol.* 20 (1986) 472–481.
- [26] T.J. Jentsch, W. Gunther, Chloride channels: an emerging molecular picture, *Bioessays* 19 (1997) 117–126.
- [27] M. Kawasaki, S. Uchida, T. Monkawa, A. Miyawaki, K. Mikoshiba, F. Marumo, S. Sasaki, Cloning and expression of a protein kinase C-regulated chloride channel abundantly expressed in rat brain neuronal cells, *Neuron* 12 (1994) 597–604.
- [28] M.C. Koch, K. Steinmeyer, C. Lorenz, K. Ricker, F. Wolf, M. Otto, B. Zoll, F. Lehmann-Horn, K.H. Grzeschik, T.J. Jentsch, The skeletal muscle chloride channel in dominant and recessive human myotonia, *Science* 257 (1992) 797–800.
- [29] U. Kornak, D. Kasper, M.R. Bosl, E. Kaiser, M. Schweizer, A. Schulz, W. Friedrich, G. Delling, T.J. Jentsch, Loss of the ClC-7 chloride channel leads to osteopetrosis in mice and man, *Cell* 104 (2001) 205–215.
- [30] R. Lalonde, Motor abnormalities in weaver mutant mice, *Exp. Brain Res.* 65 (1987) 479–481.
- [31] F. Lamb, G. Clayton, B. Liu, R. Smith, T. Barna, B. Schutte, Expression of CLCN voltage-gated chloride channel genes in human blood vessels, *J. Mol. Cell. Cardiol.* 31 (1999) 657–666.
- [32] Y. Levkovitz, E. Avignone, Y. Groner, M. Segal, Upregulation of GABA neurotransmission suppresses hippocampal excitability and prevents long-term potentiation in transgenic superoxide dismutase-overexpressing mice, *J. Neurosci.* 19 (1999) 10977–10984.
- [33] J. Lewis, E. McGowan, J. Rockwood, H. Melrose, P. Nacharaju, M. Van Slegtenhorst, K. Gwinn-Hardy, M. Paul Murphy, M. Baker, X. Yu, K. Duff, J. Hardy, A. Corral, W.L. Lin, S.H. Yen, D.W. Dickson, P. Davies, M. Hutton, Neurofibrillary tangles, amyotrophy and progressive motor disturbance in mice expressing mutant (P301L) tau protein, *Nat. Genet.* 25 (2000) 402–405.
- [34] X. Li, K. Shimada, L.A. Showalter, S.A. Weinman, Biophysical

- properties of CIC-3 differentiate it from swelling-activated chloride channels in CHO-K1 cells, *J. Biol. Chem.* 275 (2000) 35994–35998.
- [35] X. Li, T. Wang, Z. Zhao, S.A. Weinman, The CIC-3 chloride channel promotes acidification of lysosomes in CHO-K1 and Huh-7 cells, *Am. J. Physiol. Cell. Physiol.* 282 (2002) C1483–C1491.
- [36] W. Loscher, B. Nolting, The role of technical, biological and pharmacological factors in the laboratory evaluation of anticonvulsant drugs. IV. Protective indices, *Epilepsy Res.* 9 (1991) 1–10.
- [37] E.W. Lothman, Pathophysiology of seizures and epilepsy in the mature and immature brain: cells, synapses and circuits, in: W.E. Dodson, J.M. Pellock (Eds.), *Pediatric Epilepsy: Diagnosis and Therapy*, Demo Publications, New York, 1993, pp. 1–15.
- [38] T. Ogura, T. Furukawa, T. Toyozaki, K. Yamada, Y.J. Zheng, Y. Katayama, H. Nakaya, N. Inagaki, CIC-3B, a novel CIC-3 splicing variant that interacts with EB50 and facilitates expression of CFTR-regulated ORCC, *FASEB J.* 16 (2002) 863–865.
- [39] K. Oguro, N. Oguro, T. Kojima, S.Y. Grooms, A. Calderone, X. Zheng, M.V. Bennett, R.S. Zukin, Knockdown of AMPA receptor GluR2 expression causes delayed neurodegeneration and increases damage by sublethal ischemia in hippocampal CA1 and CA3 neurons, *J. Neurosci.* 19 (1999) 9218–9227.
- [40] R.W. Olsen, T.M. DeLorey, GABA and glycine, in: B.W.A.G.J. Siegel, R.W. Albers, S.K. Fisher, M.D. Uhler (Eds.), *Basic Neurochemistry: Molecular, Cellular and Medical Aspects*, 6th Edition, Lippincott-Raven, Philadelphia, PA, 1999, pp. 335–346, Chapter 16.
- [41] S. Palmer, J. Perry, A. Ashworth, A contravention of Ohno's law in mice, *Nat. Genet.* 10 (1995) 472–476.
- [42] T.M. Pham, J.C. Lacaille, Multiple postsynaptic actions of GABA via GABAB receptors on CA1 pyramidal cells of rat hippocampal slices, *J. Neurophysiol.* 76 (1996) 69–80.
- [43] N. Piwon, W. Gunther, M. Schwake, M.R. Bosl, T.J. Jentsch, CIC-5 Cl⁻ channel disruption impairs endocytosis in a mouse model for Dent's disease, *Nature* 408 (2000) 369–373.
- [44] R.J. Reimer, E.A. Fon, R.H. Edwards, Vesicular neurotransmitter transport and the presynaptic regulation of quantal size, *Curr. Opin. Neurobiol.* 8 (1998) 405–412.
- [45] C.E. Ribak, P.H. Tran, I. Spigelman, M.M. Okazaki, J.V. Nadler, Status epilepticus-induced hilar basal dendrites on rodent granule cells contribute to recurrent excitatory circuitry, *J. Comp. Neurol.* 428 (2000) 240–253.
- [46] C. Rivera, J. Voipio, J.A. Payne, E. Ruusuvoori, H. Lahtinen, K. Lamsa, U. Pirvola, M. Saarma, K. Kaila, The K⁺/Cl⁻ co-transporter KCC2 renders GABA hyperpolarizing during neuronal maturation, *Nature* 397 (1999) 251–255.
- [47] R. Sah, R.D. Schwartz-Bloom, Optical imaging reveals elevated intracellular chloride in hippocampal pyramidal neurons after oxidative stress, *J. Neurosci.* 19 (1999) 9209–9217.
- [48] S. Schmieder, S. Lindenthal, J. Ehrenfeld, Tissue-specific N-glycosylation of the CIC-3 chloride channel, *Biochem. Biophys. Res. Commun.* 286 (2001) 635–640.
- [49] B.C. Schutte, B. Yang, L.W. Dickerson, R.A. Williamson, F.S. Lamb, Clc3 knockout mice are small, exhibit kyphoscoliosis, and die prematurely, *FASEB J.* 14 (2000) A54.
- [50] R.L. Smith, G.H. Clayton, C.L. Wilcox, K.W. Escudero, K.J. Staley, Differential expression of an inwardly rectifying chloride conductance in rat brain neurons: a potential mechanism for cell-specific modulation of postsynaptic inhibition, *J. Neurosci.* 15 (1995) 4057–4067.
- [51] R.F. Squires, E. Saederup, J.N. Crawley, P. Skolnick, S.M. Paul, Convulsant potencies of tetrazoles are highly correlated with actions on GABA/benzodiazepine/picrotoxin receptor complexes in brain, *Life Sci.* 35 (1984) 1439–1444.
- [52] K. Staley, R. Smith, A new form of feedback at the GABA(A) receptor, *Nat. Neurosci.* 4 (2001) 674–676.
- [53] K. Staley, R. Smith, J. Schaack, C. Wilcox, T.J. Jentsch, Alteration of GABAA receptor function following gene transfer of the CLC-2 chloride channel, *Neuron* 17 (1996) 543–551.
- [54] K.J. Staley, B.L. Soldo, W.R. Proctor, Ionic mechanisms of neuronal excitation by inhibitory GABAA receptors, *Science* 269 (1995) 977–981.
- [55] K. Steinmeyer, B. Schwappach, M. Bens, A. Vandewalle, T.J. Jentsch, Cloning and functional expression of rat CLC-5, a chloride channel related to kidney disease, *J. Biol. Chem.* 270 (1995) 31172–31177.
- [56] O. Steward, Topographic organization of the projections from the entorhinal area to the hippocampal formation of the rat, *J. Comp. Neurol.* 167 (1976) 285–314.
- [57] O. Steward, S.A. Scoville, Cells of origin of entorhinal cortical afferents to the hippocampus and fascia dentata of the rat, *J. Comp. Neurol.* 169 (1976) 347–370.
- [58] S.M. Stobrawa, T. Breiderhoff, S. Takamori, D. Engel, M. Schweizer, A.A. Zdebik, M.R. Bosl, K. Ruether, H. Jahn, A. Draguhn, R. Jahn, T.J. Jentsch, Disruption of CIC-3, a chloride channel expressed on synaptic vesicles, leads to a loss of the hippocampus, *Neuron* 29 (2001) 185–196.
- [59] J.L. Stringer, Pentylentetrazol elicits epileptiform activity in the dentate gyrus of the urethane anesthetized rat by activation of the entorhinal cortex, *Brain Res.* 636 (1994) 221–226.
- [60] M. Takumida, D. Bagger-Sjoberg, H. Rask-Andersen, The endolymphatic sac and inner ear homeostasis. II: Effect of glycerol on the sensory end organs with or without colchicine pretreatment, *Hear. Res.* 40 (1989) 17–28.
- [61] S.M. Thompson, Modulation of inhibitory synaptic transmission in the hippocampus, *Prog. Neurobiol.* 42 (1994) 575–609.
- [62] R.J. Turner, J.N. George, B.J. Baum, Evidence for a Na⁺/K⁺/Cl⁻ cotransport system in basolateral membrane vesicles from the rabbit parotid, *J. Membr. Biol.* 94 (1986) 143–152.
- [63] W. Van Paesschen, T. Revesz, J.S. Duncan, M.D. King, A. Connelly, Quantitative neuropathology and quantitative magnetic resonance imaging of the hippocampus in temporal lobe epilepsy, *Ann. Neurol.* 42 (1997) 756–766.
- [64] S.U. Walkley, P.A. March, C.E. Schroeder, S. Wurzelmann, R.D. Jolly, Pathogenesis of brain dysfunction in Batten disease, *Am. J. Med. Genet.* 57 (1995) 196–203.
- [65] S.S. Wang, O. Devuyst, P.J. Courtoy, X.T. Wang, H. Wang, Y. Wang, R.V. Thakker, S. Guggino, W.B. Guggino, Mice lacking renal chloride channel, CLC-5, are a model for Dent's disease, a nephrolithiasis disorder associated with defective receptor-mediated endocytosis, *Hum. Mol. Genet.* 9 (2000) 2937–2945.
- [66] K.H. Weylandt, M.A. Valverde, M. Nobles, S. Raguz, J.S. Amey, M. Diaz, C. Nastrucci, C.F. Higgins, A. Sardini, Human CIC-3 is not the swelling-activated chloride channel involved in cell volume regulation, *J. Biol. Chem.* 276 (2001) 17461–17467.
- [67] M.P. Witter, A survey of the anatomy of the hippocampal formation, with emphasis on the septotemporal organization of its intrinsic and extrinsic connections, *Adv. Exp. Med. Biol.* 203 (1986) 67–82.
- [68] M.P. Witter, F.G. Wouterlood, P.A. Naber, T. Van Haeften, Anatomical organization of the parahippocampal–hippocampal network, *Ann. N. Y. Acad. Sci.* 911 (2000) 1–24.
- [69] H.Q. Wu, R. Schwarcz, Focal microinjection of gamma-acetylenic GABA into the rat entorhinal cortex: behavioral and electroencephalographic abnormalities and preferential neuron loss in layer III, *Exp. Neurol.* 153 (1998) 203–213.
- [70] K. Yamada, S. Goto, Y. Ushio, Occurrence of heat shock response in deafferented neurons in the substantia nigra of rats, *Neuroscience* 62 (1994) 793–801.
- [71] H.Z. Yin, S.L. Sensi, S.G. Carriedo, J.H. Weiss, Dendritic localization of Ca(2+)-permeable AMPA/kainate channels in hippocampal pyramidal neurons, *J. Comp. Neurol.* 409 (1999) 250–260.
- [72] M. Yoshikawa, S. Uchida, J. Ezaki, T. Rai, A. Hayama, K. Kobayashi, Y. Kida, M. Noda, M. Koike, Y. Uchiyama, F. Marumo, E. Kominami, S. Sasaki, CLC-3 deficiency leads to phenotypes similar to human neuronal ceroid lipofuscinosis, *Genes Cells* 7 (2002) 597–605.